sustainability

MDPI

Article

Real-Time Dynamic Train Dispatching for Sustainable and Energy-Efficient Operations: An Automata-Based Receding Horizon Control Framework

Yan Xu [1,2], Wei She [1], Wending Xie [1] and Yan Zhuang [1,*]

[1] School of Computer Science and Artificial Intelligence, Zhengzhou University, Zhengzhou 450001, China; wshe@zzu.edu.cn (W.S.); xwd@gs.zzu.edu.cn (W.X.)
[2] School of Transportation Management, Zhengzhou Railway Vocational & Technical College, Zhengzhou 451460, China
* Correspondence: yan.zhuang@zzu.edu.cn; Tel.: +86-15237182896

Abstract

Improving energy efficiency is critical for the sustainable development of urban public transportation. Regenerative braking is widely employed in urban rail transit to recycle braking kinetic energy into the traction network, thereby enhancing system efficiency. However, without effective scheduling, excessive feedback energy can induce instantaneous voltage spikes, leading to line overheating and accelerated equipment aging. Existing studies often fail to fully address these challenges due to simplified physical models and limited adaptability to real-time environments. To overcome these limitations, this study proposes a dynamic scheduling method for the efficient utilization of regenerative energy within a train fleet. A physical simulation system featuring a "Network-Train-Control" three-layer architecture is constructed. By formally describing the physical coupling among network topology, operational rules, and train kinematics, the system enables accurate energy profiling under realistic impedance and signaling constraints. Furthermore, a finite state automaton (FSA) is utilized to abstract continuous train dynamics into discrete states, facilitating a braking-event-triggered Model Predictive Control (MPC) framework. This framework predicts and dynamically adjusts fleet operations within a receding horizon to maximize the immediate absorption of regenerative energy. Experimental results demonstrate that the proposed method achieves active energy cooperation among trains, increasing the regenerative energy utilization rate by approximately 11%, thereby offering a viable technical solution for low-carbon urban transit.

Keywords: urban rail transit; regenerative braking energy; sustainability; real-time dispatching; automata; Model Predictive Control

Check for updates

Academic Editor: Haodong Yin

Received: 11 January 2026
Revised: 27 January 2026
Accepted: 5 February 2026
Published: 8 February 2026

Copyright: © 2026 by the authors. Licensee MDPI, Basel, Switzerland. This article is an open access article distributed under the terms and conditions of the Creative Commons Attribution (CC BY) license.

1. Introduction

As the mid-21st century approaches, global urbanization has entered a phase of unprecedented acceleration. The continuous agglomeration of populations within metropolitan areas compels nations worldwide to re-evaluate the carrying capacity of their transportation infrastructure. Against this backdrop, urban rail transit (URT)—distinguished by its high capacity, operational efficiency, and low carbon footprint—has emerged as a pivotal solution to the twin challenges of traffic congestion and environmental degradation in megacities.

This trajectory is vividly underscored by statistical data from 2024. Globally, the expansion of URT networks has not decelerated in the face of economic fluctuations; on the contrary, governments have intensified infrastructure investments to bolster economic recovery and facilitate a green transition. Statistics indicate that in 2024 alone, approximately 1300 km of new metro lines were commissioned worldwide [1].

However, the rapid expansion of the network has been accompanied by an exponential increase in energy consumption. Although urban rail transit systems exhibit superior per capita energy efficiency compared to other transportation modes, their massive operational scale has transformed them into significant loads on urban power grids. Analysis of operational data reveals that electricity consumption constitutes a substantial proportion of operating costs. Consequently, against the backdrop of fluctuating energy prices and mounting global pressure for carbon emissions reduction, enhancing energy efficiency is no longer merely a technical optimization metric, but a critical imperative for environmental sustainability.

Traction energy consumption accounts for 40% to 50% of the total electricity usage of metro lines [2]. This high proportion is primarily attributed to the frequent acceleration and braking cycles resulting from the high-density station layout in urban areas [2]. The operational profile of metro trains typically comprises four phases: acceleration, cruising, coasting, and braking. Among these, the acceleration phase represents the primary stage of energy consumption, where electric energy is converted into kinetic energy to overcome massive inertia and running resistance. Conversely, during the braking phase, modern metro trains universally adopt regenerative braking technology. In this mode, traction motors function as generators, converting the train's kinetic energy back into electrical energy and feeding it into the power supply network.

However, in the widely adopted DC power supply systems, traction substations are typically equipped with diode rectifiers, preventing energy from flowing back to the upstream AC grid. Consequently, the most energy-efficient scenario occurs when regenerative energy is instantaneously absorbed by other accelerating trains within the same power supply section. If no suitable recipient trains exist and the network lacks energy storage devices, the DC bus voltage will rise rapidly. Once a safety threshold is exceeded, the onboard braking chopper activates to dissipate the regenerative energy as heat through braking resistors. This process not only results in energy wastage but also imposes an additional thermal burden on the tunnel ventilation and air conditioning systems [3].

To enhance the utilization rate of regenerative braking energy, various solutions have been proposed in the literature. These are primarily categorized into two types: adding hardware infrastructure and optimizing train scheduling. Hardware-based approaches involve installing on-board energy storage systems (e.g., supercapacitors, lithium batteries) or deploying energy feedback devices (such as reversible inverters) at substations [4]. However, these solutions face high initial investment costs and significant safety and maintenance burdens. Meanwhile, wayside energy storage systems, which utilize supercapacitors or flywheel batteries to absorb surplus energy at substations and release it during traction, are subject to line transmission losses [5,6]. On-board energy storage systems mount the storage units directly on the trains, thereby eliminating transmission losses. Nevertheless, the added weight of on-board batteries increases the train's tare weight, resulting in a higher baseline for traction energy consumption, which partially negates the energy-saving benefits. In contrast, train scheduling optimization has garnered significant attention as it requires no additional equipment investment [2].

1.1. Background

Fundamentally, the URT system represents a high-dimensional, heterogeneous Cyber–Physical System (CPS), characterized by the deep coupling among infrastructure, rolling stock, and control logic. The realistic metro operational environment entails complex interactions among distributed variables, including but not limited to: the line impedance of the power supply network, train kinematics and energy consumption, stochastic fluctuations in passenger loads, and random delays arising from unexpected incidents. Consequently, under the premise of accounting for these variables and adhering to operational constraints, optimizing the regenerative braking energy (RBE) absorption of the train fleet through operational state adjustments presents significant challenges. These challenges are specifically manifested in the following system characteristics:

The mathematical modeling of train traction power involves complex physical coupling relationships and exhibits piecewise characteristics in the time domain. The actual power during train operation is not a simple function of velocity; rather, it is a complex non-linear function resulting from the real-time interaction between line infrastructure (e.g., gradient, curvature) and time-varying environmental parameters (e.g., running resistance, wheel-rail adhesion coefficients) [7–10]. Furthermore, the train's power profile is a piecewise function governed by electric motor characteristics, where the power functions differ significantly across various operational states. To achieve efficient absorption of RBE, it is insufficient to consider simple temporal alignment. Instead, the analysis of RBE absorption efficiency must be conducted separately according to the distinct electrical characteristics of the power function's different stages. This approach allows for the derivation of the globally optimal effect within the time interval where regenerative braking occurs [11,12].

The volume of train operational data is substantial, resulting in high computational complexity for real-time optimization analysis. The absorption of regenerative braking energy is realized through the coordinated operation of multiple trains; consequently, optimization decisions regarding inter-train adjustments can only be formulated when the comprehensive operational data of the entire fleet is fully captured. However, the massive scale of metro operational data makes it computationally prohibitive to derive global real-time decisions solely by analyzing the continuous characteristics of individual trains [13,14]. To achieve real-time global dispatching optimization, it is essential to construct a multi-layer simulation system that integrates physical dynamics models—fusing continuous states with discrete classifications—and decision-making algorithms. By extracting discrete state points from real-time operational data while preserving critical features of continuous train motion, this approach provides a rigorous physical basis for global energy optimization algorithms. This enables the mapping from continuous variables to controllable events, thereby supporting the generation of real-time decisions [15–19].

Train operations require the efficient synergy of global planning and local real-time adjustments under strict multiple constraints [20,21]. During operation, trains receive dispatching commands from the control center; these commands must be executed subject to fleet-wide operational rules to prevent line conflicts. Simultaneously, trains receive real-time information from the signaling system and must respond promptly to adjustment directives [22,23]. To ensure operational safety and efficiency, the system must perform multi-objective dynamic optimization during the response process. This entails rapidly identifying an optimal or feasible solution among multiple conflicting objectives, including conflict avoidance, adherence to timetable targets, and compliance with physical and regulatory constraints. Furthermore, all adjustment decisions must be formulated from a fleet coordination perspective. Any command directed at a single train should be assessed for potential knock-on effects to preclude global disturbances within the system [24,25].

Train timetable optimization is widely recognized as a cost-effective strategy for energy conservation. However, a critical gap persists between existing theoretical models and the physical realities of train operation scenarios. Although previous studies have demonstrated effectiveness under idealized conditions, they predominantly rely on static scheduling strategies or continuous function approximations. Consequently, these approaches are ill-suited to address the high-dimensional coupling and stochastic constraints inherent in actual train dynamics. In light of this, this paper analyzes the limitations of current methodologies and proposes targeted solutions structured around the following three aspects:

1. Optimization misjudgments caused by simplified train power models. In an effort to alleviate computational burdens, early studies (e.g., Ramos [26]) approximated traction and braking power profiles as rectangular waves or binary states (0/1). This approximation transforms the intricate problem of energy integration into a geometric problem focusing on maximizing "time overlap," thereby overlooking the non-linear amplitude characteristics of power curves. Subsequent research by Yang et al. [27] indicated that maximizing temporal overlap does not equate to maximizing energy exchange. For example, rectangular models may align the final phase of braking (a low-power region) with the initial phase of traction (similarly a low-power region); despite the temporal alignment, the actual energy exchange is minimal. In contrast, an effective energy-saving strategy requires a method that aligns the peak braking power interval (typically during high-speed braking) with the constant traction power interval, flexibly maximizing the overlap of power magnitudes rather than just durations based on train operation states.
2. Reliance on continuous function models failing to meet discrete control requirements. The mathematical optimization models adopted by scholars such as Ran [28] typically formulate train kinematics and power profiles as continuously differentiable functions. However, this assumption fails to capture the discrete control characteristics of practical train systems. Consequently, it is essential to establish an event-driven modeling approach. Specifically, this approach employs train state transition events as core variables to construct a scheduling strategy capable of responding to discrete state inputs [29,30]. This methodology ensures that optimization decisions are directly mapped to executable control commands, thereby maximizing the spatiotemporal synergy efficiency of energy between traction and braking processes [31].
3. Static open-loop models lacking dynamic adjustment capabilities. Studies by scholars such as Yang [32] predominantly employ offline global optimization methods to generate static train timetables. However, metro operations are inherently stochastic systems. Disturbances such as dwell time fluctuations and signal delays trigger the accumulation of errors, causing static timetables to become obsolete within minutes of operation. Given the inability of static models to effectively mitigate real-time perturbations, there is a critical need to construct a proactive closed-loop control framework. This framework must possess receding horizon prediction capabilities, allowing it to generate coordinated train adjustment strategies based on real-time states. Consequently, this approach achieves the optimization of dynamic energy interactions under stochastic conditions.

1.2. Contribution

To address the limitations regarding the oversimplified physical models and the insufficient adaptability of static scheduling in existing research, this paper proposes a real-time dynamic dispatching method tailored for the energy synchronization of train groups. This method constructs a 3-layer physical simulation system for urban rail transit to acquire

train operational states. By utilizing a Model Predictive Control rolling horizon framework based on automata theory to continuously predict braking power data and optimize operational trajectories in real-time, the proposed approach achieves the optimization of the regenerative braking energy utilization rate. The main contributions of this paper are summarized as follows :

1. Construction of a Spatiotemporal Simulation Architecture. Architecture Based on a physical simulation environment, this study establishes a simulation system integrating a 3-layer architecture: network-level, train-level, and bogie-control-level. The system formally characterizes the physical coupling relationships among the spatial topology of the network, operational rules, and train kinematics within urban rail transit. This system not only accurately reproduces the operational behaviors of train groups subject to actual line impedance and signaling system constraints but also generates precise energy consumption curves that fully account for the nonlinear characteristics of the power supply network, thereby enabling the validation of the effectiveness of energy-saving-oriented dispatching strategies.The fundamental novelty lies in the FSA-based dynamic interface, which acts as a real-time bridge to map continuous train kinematics into discrete control states. This mechanism enables the MPC to actively modulate the network-level energy flow based on real-time physical feedback, distinguishing it from conventional static or open-loop hierarchical frameworks.
2. Discretization of Physical Models via Hybrid Automata Modeling. In response to the computational complexity inherent in train control systems, this study proposes a finite automata-based modeling approach that abstracts continuous train dynamics into sequences of discrete states. Through the extraction of operational states from the 3-layer architecture, the train operation process is encoded as a finite state flow graph. This abstraction effectively converts the conventional continuous control problem into a parameter optimization problem concerning switching instants.
3. Formulation of a Dynamic MPC Framework for Regenerative Braking Energy Synchronization. This research utilizes a finite automata model to characterize the diverse operational modes (traction, coasting, and braking) and associated state transitions of the train. The framework incorporates a braking-event-triggered MPC scheme that dynamically modulates dwell times to maximize the absorption and utilization of regenerative braking energy. Leveraging a Rolling Horizon Control mechanism, the MPC allows for the rectification of current state deviations while proactively anticipating future energy synchronization windows. This approach facilitates proactive energy recovery and significantly bolsters system robustness in the presence of stochastic disturbances.

2. Mathematical Model and Approach

2.1. Urban Rail Transit Simulation System

This study establishes an integrated Network-Train-Bogie three-layer architecture at the system level. This framework constructs a high-dimensional and tightly coupled parameter space that encompasses track conditions, vehicle dynamics, and motor characteristics. As shown in Figure 1, the interaction between parameter transmission and state feedback is realized through a mechanism combining centralized schedule dispatching with real-time feedback from multi-train model entities.

The Network Layer defines the spatiotemporal framework and formulates global dispatching protocols for the train fleet. Temporal parameters encompass the operational window from the first to the last train, station dwell times, and inter-station travel times. Geospatial parameters specify station coordinates and section mileages, while simultaneously acquiring real-time train positioning data . Furthermore, this layer governs fleet

scheduling rules, including the number of dispatched trains, departure sequence, headway requirements, and turnaround strategies.

The Train Layer generates continuous trajectory profiles for individual trains by constructing a longitudinal dynamics model. By integrating physical factors such as total train mass, aerodynamic drag, rolling resistance, and track gradient, this model computes the target operation curve based on specific driving strategies and track conditions. The resulting output delineates the coupling relationship among velocity, time, and position.

The Bogie Layer calculates the precise power output profile for individual trains. It dynamically inputs the operational states derived from the Train Layer into an inverter-motor model. This model generates a real-time electrical response based on the torque and rotational speed requirements of the traction system, thereby producing a traction power curve that is strictly synchronized with the kinematic behavior defined in the train-level model.

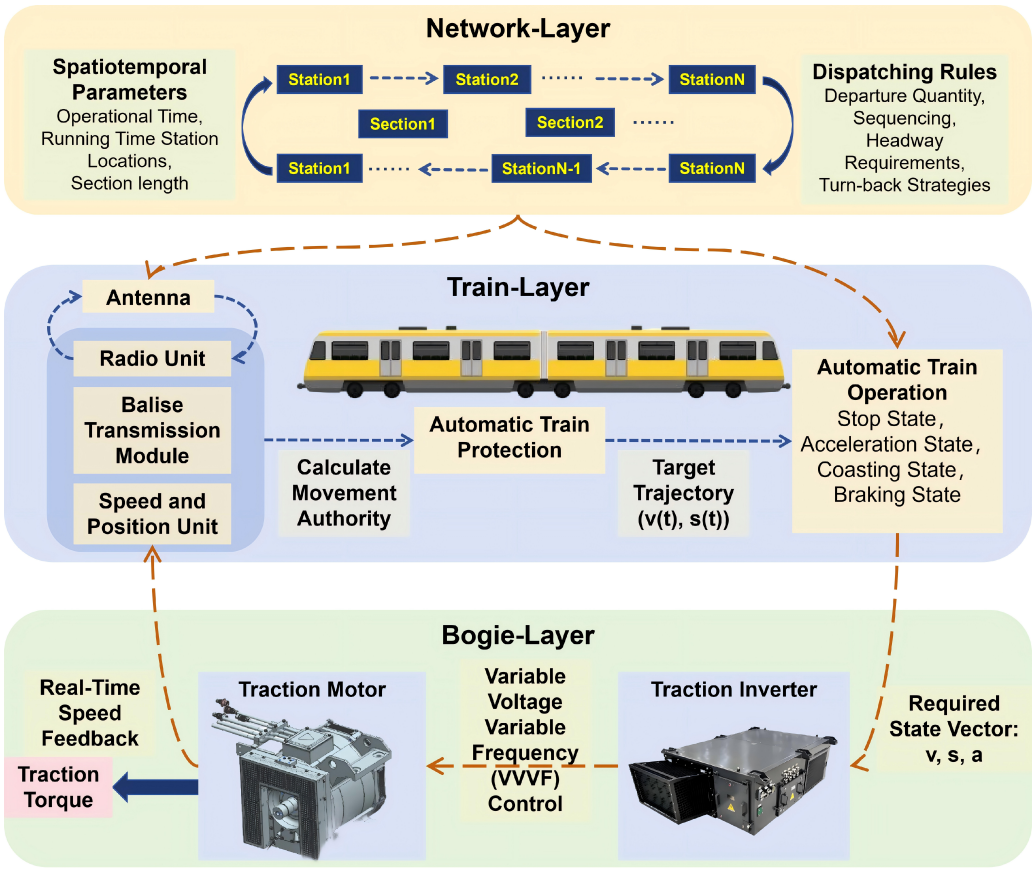

Figure 1. Network-Train-Bogie Three-layer Architecture.

2.1.1. Network-Layer Formal Modeling Framework

To comprehensively and accurately characterize the functions of the dispatching center, the network-level model defines the spatiotemporal parameters and associated operational rules. The metro dispatching center establishes the start and end times of daily operations and the deployment of rolling stock, taking responsibility for compiling the daily train timetable. All trains are dispatched sequentially in accordance with the predetermined schedule. During operation, trains adhere to the arrival and departure times prescribed by the dispatching center while continuously transmitting real-time operational data—such as velocity and position—back to the center. Consequently, the dispatching center monitors the operational status in real-time and issues temporary dispatching commands to the trains based on the global traffic situation of the line.

1. Definition of Temporal Parameters

The system establishes a framework of temporal parameters for urban rail transit operations.

Operational Time: The total operation time, denoted as T_{op}, comprises peak periods T_{peak} and off-peak periods $T_{off-peak}$. The number of trains deployed for operation varies across these different periods.

Running Time: The inter-station running time $T_{run,i}$ represents the duration required for a train to travel from station i to station $i+1$.

Arrival and Departure: For train j, the arrival time at station i is denoted as $t_{arr\{i,j\}}$, and the departure time is denoted as $t_{dep\{i,j\}}$.

Dwell Time: The planned dwell time of train j at station i is $T_{\{i,j\}}$. This duration may be adjusted to a new dwell time, $T^{new}_{\{i,j\}}$, due to perturbations from passenger boarding or instructions received from the signaling system, as described in Equation (1). The range of this adjustment is constrained by lower and upper bounds determined by factors such as passenger alighting/boarding and station operations, as formulated in Equation (2).

$$T^{new}_{\{i,j\}} = T_{\{i,j\}} + \Delta t_{\{i,j\}} \tag{1}$$

$$T_{\{i,\min\}} \le T^{new}_{\{i,j\}} \le T_{\{i,\max\}} \tag{2}$$

Turnaround Time: The turnaround time, T_{turn}, refers to the transitional operational time after a train arrives at the terminal station and before it executes the reverse run. This duration, combined with the inter-station running times and station dwell times, constitutes the complete operational cycle of the train.

Train Operation Rules: The train operation logic is based on a fixed departure headway, $T_{interval}$. A recursive relationship is employed to systematically generate the arrival and departure schedules for all trains at every station.

Origin Station Rule: The departure time of train j at the origin station is determined by the departure time of the first train, T_{first}:

$$t_{arr\{1,j\}} = t_{dep\{1,j\}} = T_{first} + (j-1)T_{interval} \tag{3}$$

Subsequent Station Rule: The arrival time $t_{arr\{i,j\}}$ and departure time $t_{dep\{i,j\}}$ of the train at a subsequent station i are jointly determined by its departure time from the preceding station, the inter-station running time $T_{run,i-1}$, and the dwell time $T_{\{i,j\}}$ at the current station:

$$\begin{aligned} t_{arr\{i,j\}} &= t_{dep\{i-1,j\}} + T_{run,i-1} \\ t_{dep\{i,j\}} &= t_{arr\{i,j\}} + T_{\{i,j\}} \end{aligned} \tag{4}$$

Terminal Station Rule: At the terminal station, the model incorporates the turnaround time T_{turn} to calculate the departure time for the return direction:

$$t_{dep\{n,j\}} = t_{arr\{n,j\}} + T_{turn} \tag{5}$$

2. Definition of Spatial Parameters

The set of station locations in the urban rail transit system, denoted as O, serves as a mathematical abstraction of the physical spatial positions of the stations. It characterizes the sequential position of each station within the line as well as its directional attribute. The expression is given by $O = \{o_i | o_i = (s_i, d_i)\}$. Here, s_i represents the station sequence number, which explicitly distinguishes the chronological order of different stations along the entire line through a sequence of positive integers, serving as the fundamental identifier for train positioning and dispatching. The variable

$d_i \in \{up, down\}$ denotes the directional attribute, corresponding to the "up" direction (forward travel along the line) and the "down" direction (reverse travel), respectively. The bidirectional symmetry is formalized through an inverse mapping function ψ. For any upstream station sequence $S_{up} = [s_1, s_2, \cdots, s_n]$, the corresponding downstream sequence is consistently defined as $S_{down} = \psi(S_{up})$. The section object function $X(s_i, s_{i+1}) = s_i \oplus s_{i+1}$ generates a globally unique section identifier by connecting the codes of adjacent stations. The railway line is discretized into a series of segments using the stations as boundaries. The total length of the entire section, denoted as L_{total}, is defined as the sum of the lengths of all segments:

$$L_{total} = \sum_{i=1}^{n} l_i \tag{6}$$

The cumulative length functions for the up and down directions adopt the asymmetric definitions $L_{up}(e)$ and $L_{down}(e)$, respectively. They accumulate the segment lengths l_i starting from the origin of their respective directions. This approach precisely characterizes the spatial asymmetry caused by line geometry (such as gradient and curvature) during bidirectional operation, providing a critical spatial baseline for the subsequent calculation of running resistance and traction energy consumption.

2.1.2. Train-Layer Dynamics Model

To define the global operational state of the train, let the physical state of the train within an operation cycle T_{global} be denoted as a continuous vector function $\Psi(t)$:

$$\Psi(t) = [s(t), v(t), a(t), P(t), u(t)]^T, \quad t \in T_{global} \tag{7}$$

where:

- $s(t)$, $v(t)$, and $a(t)$ represent the position, velocity, and acceleration functions, respectively;
- $P(t)$ denotes the power function (defined as positive for traction and negative for braking, or defined separately);
- $u(t)$ represents the control command vector (used to delineate state boundaries).

By regarding the metro train as a single entity and neglecting the internal forces between carriages during dynamics modeling, a force equilibrium equation is established based on Newton's Second Law, as presented in Equation (8). The active forces—namely, traction and braking forces—and the running resistance (encompassing aerodynamic resistance, rolling resistance, and gradient resistance, etc.) are correlated with the train's mass and acceleration for the solution. Through numerical integration of this equation of motion, the varying motion state of the train with respect to time and distance can be precisely calculated.

$$M(1+\gamma)\frac{dv}{dt} = F_{traction}(v) + F_{brake}(v) - \sum F_{resistance}(v, s) \tag{8}$$

where:

- M represents the total mass of the train (unit: kg). This value encompasses not only the tare weight of the vehicle itself but also the payload, including passengers and cargo;
- $v(t)$ denotes the instantaneous velocity of the train (m/s);
- γ is the rotary mass factor, used to correct for the rotational inertia of the wheelsets and motor rotors;
- $F_{traction}$ stands for the traction force (defined as a positive value, unit: N);

- F_{brake} represents the braking force (defined as a negative value, unit: N);
- $\sum F_{resistance}$ corresponds to the summation of all running resistances (unit: N);
- s indicates the position of the train (m).

1. Multi-source Resistance Coupling Model

The total running resistance experienced by a metro train constitutes the passive forces opposing its motion. Based on their sources and characteristics, these forces are categorized into basic running resistance and additional line resistance. The coupling of these components forms the total resistance model [33]:

$$\sum F_{resistance}(v, s) = F_{basic}(v) + F_{grade}(s) + F_{curve}(s) + F_{tunnel}(v) \tag{9}$$

(a) Basic Running Resistance

The basic running resistance is modeled using the Davis formula, expressed as:

$$F_{basic}(v) = a + bv + cv^2 \tag{10}$$

where a, b, and c are resistance coefficients determined through experimental data fitting [34]:

- Coefficient a (N): Represents the rolling friction term, which is independent of velocity.
- Coefficient b ($\mathrm{N \cdot s/m}$): Represents the term linearly related to velocity, typically accounting for mechanical bearing friction and low-speed aerodynamic effects.
- Coefficient c ($\mathrm{N \cdot s^2/m^2}$): Represents the aerodynamic drag term, which is proportional to the square of the velocity.

(b) Additional Line Resistance

Grade Resistance (F_{grade}): When the train operates on a gradient, resistance is generated by the component of gravity parallel to the track direction [35]. Let θ denote the gradient angle. Applying the approximation $\sin\theta \approx \tan\theta = i/1000$, the grade resistance is calculated as:

$$F_{grade}(s) \approx Mg \cdot \frac{i(s)}{1000} \tag{11}$$

where M is the train mass, g is the gravitational acceleration, and $i(s)$ represents the gradient value (in permille) at position s.

Curve Resistance (F_{curve}): When the train traverses a curved section, resistance increases due to a series of complex phenomena, including friction between the wheel flange and the inner rail caused by centrifugal force, as well as longitudinal and lateral wheel slippage [36]. This is defined as:

$$F_{curve}(s) = \frac{C}{R} \tag{12}$$

where R is the curve radius and C is an empirical coefficient specific to the rolling stock and track conditions.

Tunnel Aerodynamic Resistance (F_{tunnel}) Upon entering a tunnel, the train's aerodynamic environment undergoes a drastic change. The confined space between the train body and the tunnel walls causes severe air compression and acceleration, generating a "piston effect" that significantly amplifies aerodynamic resistance. This is approximated by [37]:

$$F_{tunnel}(v) \approx dv^3 \tag{13}$$

2. Dynamic Analysis of Train Operation States

The operation process of urban rail transit trains can be decomposed into a sequence of fundamental states: station stop, acceleration, coasting, and braking. The core model is founded on Newton's Second Law and incorporates a rotating mass factor to accurately reflect the inertial effects of the drive system [38].

Station Stop State: When the train reaches the designated stopping point at a station, its velocity decreases to zero, and it remains stationary. This condition is defined as the station stop state. During this state, the braking system continuously provides sufficient static friction to prevent rolling [39]. Currently, compressed air holding brakes (pneumatic braking) are predominantly used for this purpose rather than electric braking. The dynamics are described by:

$$\begin{cases} F_{traction} = 0, \quad F_{brake} = 0 \\ \frac{dv}{dt} = 0 \end{cases} \tag{14}$$

Acceleration State: Upon receiving the departure signal, the train departs from the station, and its velocity gradually increases from zero. Based on the characteristics of the traction motor, the acceleration phase typically transitions through constant torque acceleration, constant power acceleration, and natural characteristic regions. (See the traction control section for detailed analysis).The equations of motion are:

$$\begin{cases} F_{traction} \geq 0, \quad F_{brake} = 0 \\ \frac{dv}{dt} = \frac{F_{traction}(v) - \sum F_{resistance}(v,s)}{M(1+\gamma)} \geq 0 \end{cases} \tag{15}$$

Coasting State: Once the train reaches the designed maximum velocity, the traction power is cut off, and no electric braking is applied. The train coasts forward relying on its own inertia. Due to the presence of running resistance, the train's velocity gradually decreases.The dynamics are expressed as:

$$\begin{cases} F_{traction} = 0, \quad F_{brake} = 0 \\ \frac{dv}{dt} = \frac{-\sum F_{resistance}(v,s)}{M(1+\gamma)} < 0 \end{cases} \tag{16}$$

Braking State: When the train exceeds a set speed limit or approaches a stopping point, deceleration is initiated to reduce the speed to zero as required. Currently, electric braking is commonly employed, where the traction motor switches to generator mode, converting the train's kinetic energy into regenerative braking energy. The dynamics are described by:

$$\begin{cases} F_{traction} = 0, \quad F_{brake} < 0 \\ \frac{dv}{dt} = \frac{F_{brake}(v) - \sum F_{resistance}(v,s)}{M(1+\gamma)} < 0 \end{cases} \tag{17}$$

2.1.3. Bogie-Layer Energy Consumption Model

The acceleration phase of urban rail transit trains necessitates overcoming various motion resistances, a process characterized by significant energy consumption. Electrical energy drawn from the catenary is converted into mechanical energy through key components, including the traction inverter and the electric motor. Conversely, during the braking phase, the energy flow is reversed; the traction motor transitions to a generator mode, converting the train's kinetic energy into regenerative electrical energy.

The traction motor serves as the pivotal device for energy conversion within the train operation process. By analyzing the energy consumption characteristics of a single motor

and integrating the train composition (marshalling) data, an equivalent model scaling from a single motor to the entire train is established to calculate the total system energy consumption. It is noted that the total energy consumption of the train also comprises auxiliary equipment powered by batteries and other sources; however, this portion is excluded from the scope of the present discussion.

The energy conversion within the traction system involves multiple components, including the line filter, traction inverter, traction motor, and mechanical transmission gears. As each component introduces specific energy losses, the overall efficiency of the traction system, denoted as η_{total}, is expressed as the product of the efficiencies of these individual stages [40]:

$$\eta_{total} = \eta_{filter} \times \eta_{inv} \times \eta_{motor} \times \eta_{gear} \tag{18}$$

where:

- η_{filter}: Efficiency of the line filter and DC link circuit.
- η_{inv}: Comprehensive efficiency of the traction inverter.
- η_{motor}: Efficiency of the traction motor.
- η_{gear}: Efficiency of the mechanical transmission (gearbox).

To extend the energy consumption analysis from a single motor to the entire train, the collaborative operation of all motors in the train consist must be considered. Assuming the train is driven by N_{motor} identical asynchronous motors, the total traction force of the train can be represented as the summation of the traction forces produced by the individual motors. Based on the fundamental relationships, this is expressed as:

$$F_{traction}(v) = N_{motor} F_{motor}(v) \tag{19}$$

where:

- $F_{motor}(v)$: The traction force produced by a single motor (N) as a function of velocity.
- N_{motor}: The total number of traction motors in the train consist.

1. Modeling of Acceleration Power Characteristics
   During the acceleration phase, the traction motor operates in motoring mode, representing the primary period of energy consumption. The acceleration process is jointly constrained by the inverter's voltage and current limits, as well as the motor's electromagnetic limitations, resulting in distinct segmented characteristics. These segments are, in sequence: the Constant Torque Region, the Constant Power Region, and the Natural Characteristic Region [41].
   Energy Analysis in the Constant Torque Region ($0 \leq v \leq v_1$). To meet the demands of high-efficiency and high-density metro operations, and to ensure the train reaches a relatively high speed within the shortest possible time from a standstill, the traction motor's output torque is maintained at its maximum value, $T_m = T_{\max}$, during the initial low-speed phase. According to electric motor principles, torque is proportional to the air-gap magnetic flux. Therefore, constant torque implies constant air-gap flux. Since magnetic flux is proportional to the ratio of electromotive force (EMF) to frequency, both EMF and frequency are increased proportionally in this region to maintain constant flux. As the rotational speed increases, this region concludes when the voltage reaches its upper limit.
   In the constant torque region, the motor provides a constant torque, resulting in a constant traction force as the velocity increases from zero to the corner velocity v_1. The electrical energy absorbed is utilized to increase kinetic energy and overcome

resistance. The required traction force $F_{traction}(v)$ and the train's total traction power $P_{total,trac}(t)$ are expressed as:

$$F_{traction}(v) = NF_{\max} = N\frac{T_{\max} i_g}{r}$$

$$P_{total,trac}(t) = NF_{\max} \cdot v(t) \tag{20}$$

The total energy consumed by the traction system in the constant torque region is calculated as:

$$E_{absorb,ct} = \int_{t_1}^{t_2} \frac{NF_{\max} \cdot v(t)}{\eta_{total}} dt \tag{21}$$

In this phase, as torque remains constant, the output power increases linearly with the rise in rotational speed.

Nomenclature for this section:

- v_1: The corner velocity (or base speed) where the constant torque region ends (m/s).
- $T_{\max}$: Maximum output torque of a single motor (N · m).
- N: Total number of powered motors in the train (equivalent to N_{motor} used previously).
- i_g: Gear ratio of the transmission system.
- r: Radius of the wheel (m).
- $F_{\max}$: Maximum traction force provided by a single motor (N).
- η_{total}: Overall efficiency of the traction system.
- $E_{absorb,ct}$: Energy absorbed during the constant torque phase (J).
- t_1, t_2: The start and end times of the constant torque acceleration phase.

Energy Analysis in the Constant Power Region ($v_1 \leq v \leq v_2$).

As the motor speed continues to increase, the output voltage of the traction inverter rises until it reaches its saturation limit. Beyond this point, the voltage cannot increase synchronously with the frequency and remains clamped at its maximum value. Simultaneously, as the frequency continues to rise, the air-gap magnetic flux is forced to weaken (field weakening). Consequently, the electromagnetic torque T_m decreases inversely proportional to the motor's angular velocity ω to maintain a constant power output, defined by $P_m = T_m\omega$.

In this region, the traction force diminishes as the velocity increases [42]. Although the acceleration rate gradually declines, velocity enhancement remains efficient due to the sustained constant power input. For the train accelerating from the corner velocity v_1 to the maximum constant-power velocity v_2, the required traction force $F_{traction}(v)$ is derived as:

$$F_{traction}(v) = \frac{P_{total,trac}}{v} \tag{22}$$

where the total traction power $P_{total,trac}(t)$ is the product of the number of motors and the rated power of a single motor:

$$P_{total,trac}(t) = NP_m \tag{23}$$

The total energy absorbed by the traction system in the constant power region is obtained by integrating the power over the time interval $[t_2, t_3]$:

$$E_{absorb,cp} = \int_{t_2}^{t_3} \frac{P_{total,trac}}{\eta_{total}} dt \tag{24}$$

In this phase, energy consumption is primarily sensitive to the duration of acceleration. Extending the time spent within this velocity interval will result in a significant increase in total energy consumption.

Nomenclature for Equations (22)–(24):

- v_1, v_2: The velocity range defining the constant power region (m/s).
- $P_{total,trac}$: Total traction power of the train (W).
- P_m: Rated power of a single traction motor (W).
- N: Total number of powered motors.
- η_{total}: Overall efficiency of the traction system.
- $E_{absorb,cp}$: Energy absorbed during the constant power phase (J).
- t_2, t_3: Start and end times of the constant power acceleration phase (s).

Energy Analysis in the Natural Characteristic Region ($v_2 \leq v \leq v_{\max}$).

In this final acceleration phase, the output frequency and voltage of the traction inverter reach their maximum limits and remain constant. The motor operates along its inherent "natural mechanical characteristic curve," where the output torque is determined solely by the external load (i.e., the train's running resistance). The system eventually reaches an equilibrium between the motor's traction force and the running resistance. Typically, the train attains its design maximum velocity ($v_{\max}$) within this region [43].

In the natural characteristic region, the traction force decreases significantly as velocity increases (mathematically following an inverse-square relationship). For the train accelerating from v_2 to $v_{\max}$, the required traction force $F_{traction}$ (N) and traction power $P_{total,trac}$ (W) are modeled as:

$$F_{traction}(v) = \frac{P_{total,trac} \cdot v_2}{v^2}$$

$$P_{total,trac}(t) = \frac{P_{total,trac} \cdot v_2}{v(t)} \tag{25}$$

The total energy absorbed by the system during this interval $[t_3, t_4]$ is calculated as:

$$E_{absorb,n} = \int_{t_3}^{t_4} \frac{1}{\eta_{total}} \cdot \frac{P_{total,trac} \cdot v_2}{v} dt \tag{26}$$

The three intervals described above constitute the complete traction process for the train:

Constant Torque Region: Ensures robust starting torque and high acceleration capabilities at low speeds.

Constant Power Region: Efficiently extends the acceleration process into the medium-to-high speed range within the system's capacity constraints.

Natural Characteristic Region: Allows the train to reach and stabilize at its maximum operational velocity.

Nomenclature for Equations (25)–(26):

- $v_{\max}$: Design maximum velocity of the train (m/s).
- v_2: Velocity at the transition from the constant power region to the natural characteristic region (m/s).
- $P_{total,trac}$: The constant power value maintained during the previous region (v_1 to v_2), used here as the reference scalar (W).
- t_3, t_4: Start and end times of the natural characteristic acceleration phase (s).
- η_{total}: Overall efficiency of the traction system.

2. Modeling of Coasting Power Characteristics
During the coasting phase, the traction system is deactivated ($P_{\text{traction}} = 0$). The train overcomes running resistance relying solely on its inertia. In this stage, the energy consumption of the traction system is zero. The velocity decreases from the initial speed $v_{\max}$ to the terminal coasting speed v_3. The energy equation is expressed as:

$$E_{\text{coast}} = 0$$

3. Modeling of Regenerative Braking Power Characteristics
In this phase, the traction motor operates in generator mode, converting the train's kinetic energy into electrical energy. During the regenerative braking process, the train decelerates from v_3 to a complete standstill. The net electrical energy released is calculated by deducting the work consumed by resistance from the total kinetic energy reduction, while accounting for the regenerative braking efficiency [44].
The equation of motion is defined as:

$$F_{\text{brake}}(v) = M(1+\gamma)\frac{\mathrm{d}v}{\mathrm{d}t} + \sum F_{\text{resistance}}(v, s) \tag{27}$$

where M is the train mass and $(1+\gamma)$ represents the rotary inertia factor. The instantaneous braking power of the train, $P_{\text{total,brake}}(t)$, is given by:

$$P_{\text{total,brake}}(t) = F_{\text{brake}}(v(t)) \cdot v(t)$$

The total regenerative energy released, E_{release}, is calculated as:

$$E_{\text{release}} = \eta_{\text{return}} \int_{t_{\text{brake_start}}}^{t_{\text{stop}}} F_{\text{brake}}(v) \cdot v \, \mathrm{d}t \tag{28}$$

Here, η_{return} denotes the overall regenerative braking efficiency, which can be approximated as the product of the efficiencies of the sub-components:

$$\eta_{\text{return}} \approx \eta_{\text{motor,gen}} \cdot \eta_{\text{inv,gen}} \cdot \eta_{\text{gear,gen}} \tag{29}$$

The components of the efficiency chain are defined as follows:

- Transmission System Efficiency ($\eta_{\text{gear,gen}}$): Similar to the traction phase, mechanical energy is transmitted from the wheels to the motor shaft. Energy losses primarily occur due to gear meshing friction.
- Induction Motor Efficiency ($\eta_{\text{motor,gen}}$): The motor operates as a generator. Internal losses include copper loss, iron loss, and mechanical friction losses.
- Traction Converter Efficiency ($\eta_{\text{inv,gen}}$): The converter rectifies and stabilizes the variable-frequency, variable-voltage AC output from the motor, inverting it into a current compatible with the power grid. This power conversion process incurs switching losses and conduction losses.

2.2. FSA-Based State Extraction Model

In this study, a formal finite state automaton is constructed to characterize train operational states. The primary objective of this automaton is to resolve the mapping challenge from continuous data streams generated by the physical simulation system to discrete control logic. The proposed model decomposes the complex non-linear dynamic behaviors of the train into 4 mutually exclusive discrete modes: Stop, Accelerate, Coast, and Brake. By defining rigorous logical conditions, the automaton processes real-time continuous physical signals derived from the three-tier simulation architecture, transforming the train

states along the global time axis, denoted as T_{global}, into structured sequences of discrete states. This mechanism effectively establishes the mapping between the physical layer and the logical layer, thereby providing standardized state inputs for subsequent tasks such as circuit analysis, energy consumption calculation, and performance optimization.By explicitly defining discrete states, the FSA architecture fundamentally reduces computational complexity.

2.2.1. Formal Definition of the Automaton

Based on the operational characteristics of metro trains, a finite automaton model for train operations is constructed. It is formally defined as a 5-tuple H, as illustrated in the state automaton diagram:

$$H = (Q, \Sigma, \delta, q_1, F)$$

where:

- Q denotes the finite set of discrete states;
- Σ denotes the event and control alphabet;
- δ represents the state transition function;
- q_1 is the initial state;F is the set of final states.

1. Discrete State Set (Q)
   Q represents the finite set of discrete states corresponding to typical train operational modes, defined as the finite set $Q = \{q_1, q_2, q_3, q_4\}$. The physical definitions are as follows:
   q_1 (Station Dwell/Stop State): The train velocity is $v = 0$. Doors are open for passenger exchange. During this phase, the traction motors are disabled, and the auxiliary systems consume baseline power.
   q_2 (Traction/Acceleration State): The train draws power from the catenary system. The traction motors output a driving torque $F_{traction} > 0$, resulting in an increase in kinetic energy. This corresponds to the traction command levels of the Automatic Train Operation (ATO) system.
   q_3 (Coasting State): Both tractive force $F_{traction} = 0$ and braking force $F_{brake} = 0$. The train moves under inertia, subject only to running resistances (including basic resistance, gradient resistance, and curve resistance).
   q_4 (Braking State): Depending on the velocity and grid voltage conditions, the motors operate as generators (regenerative braking) or pneumatic braking is engaged. Kinetic energy is converted into electrical energy or thermal energy.
2. Event and Control Alphabet (Σ)
   Σ denotes the finite set of input symbols that trigger state transitions, corresponding to discrete commands from the ATO controller or internal system events. It is defined as $\Sigma = \{0, 1, 2, 3\}$, where:
   0: Hold/Parking command;
   1: Acceleration command;
   2: Power Cut-off command (transition to Coasting);
   3: Deceleration/Braking command.
3. Transition Function (δ)
   The transition function is defined as $\delta : Q \times \Sigma \to P(Q)$, characterizing the transition rules between discrete states. State transitions depend not only on the discrete control commands Σ but are also constrained by Guard Conditions ($\mathcal{G}$) derived from continuous state variables, as shown in Figure 2. The typical transition logic is described as follows:

$q_1 \rightarrow q_2$: The system transitions to the traction state upon the expiration of the dwell timer and the receipt of an acceleration command (1); otherwise, it maintains the dwell state (0).

$q_2 \rightarrow q_3$: When the train velocity reaches the preset cruising value or the energy-optimal switching point, the traction is cut off via command (2), and the system enters the coasting state.

$q_2/q_3 \rightarrow q_4$: The system enters the braking state upon receiving a braking command (3), triggered by the interception of the station-stop braking curve or the over-speed protection logic.

$q_4 \rightarrow q_1$: The system reverts to the stop state once the velocity v decreases to 0 and precise berthing is confirmed.

The detailed state transition matrix is presented in Table 1 (where $\emptyset$ denotes an undefined or invalid transition):

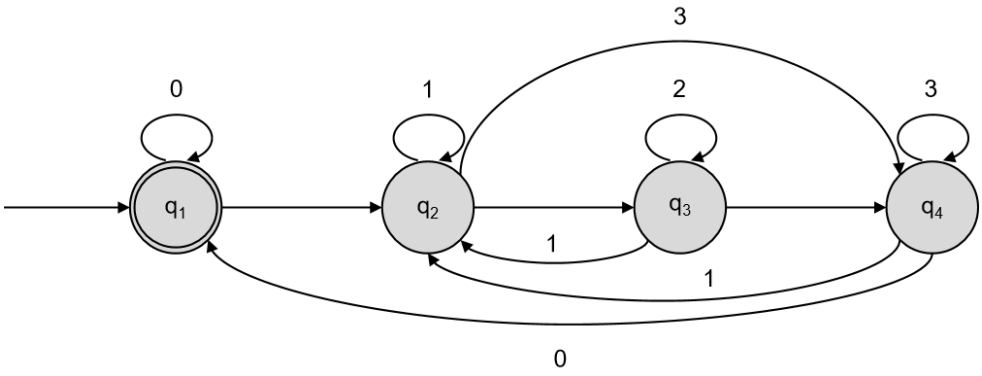

Figure 2. Network-Train-Bogie Three-layer Architecture.

Table 1. State Transition Matrix of the Train Automaton.

Current State	Input Command (Σ)			
	0 (Hold)	**1 (Accel)**	**2 (Coast)**	**3 (Brake)**
q_1 (Stop)	$\{q_1\}$	$\{q_2\}$	$\emptyset$	$\emptyset$
q_2 (Traction)	$\emptyset$	$\{q_2\}$	$\{q_3\}$	$\{q_4\}$
q_3 (Coasting)	$\emptyset$	$\{q_2\}$	$\{q_3\}$	$\emptyset$
q_4 (Braking)	$\{q_1\}$	$\{q_2\}$	$\emptyset$	$\{q_4\}$

4. Initial and Accepting States (q_{init}, F)

   q_{init}: The initial state, set as q_1, representing the train at a standstill at the departure station.

   F: The set of Accepting States, defined as $F = \{q_1\}$, representing the target state where the train has safely arrived and stopped at the next station.

2.2.2. Event Extraction Algorithm

The process of automaton-based simulation and event extraction is formally described in Algorithm 1. Initially, the raw physical operation logs are preprocessed into time-synchronized interval running data (D_{run}), and the finite automaton variables are initialized. The algorithm iteratively processes the train operation data at each time step t_k. The train status vector w serves as the input to the automaton to detect state transitions via the function δ. Upon the detection of a state transition ($S_{\text{next}} \neq S_{\text{curr}}$), a callback mechanism is triggered.

Algorithm 1 Automaton-Based Event Extraction from Operation Logs

Input: Physical Operation Log $\Psi(t)$ (trip_log), Minimum Duration Threshold τ_{min}
Output: List of Braking Events $\mathcal{E}_{j,g}$, List of Starting Events $\mathcal{E}_{j,k}$

Preprocessing: Convert $\Psi(t)$ into time-series running data $D_{run} = \{(t_k, x_k, v_k, \dots)\}_{k=1}^{N}$.
Initialize:
Current State $S_{curr} \leftarrow q_{init}$
Event Buffer $B_{temp} \leftarrow \{d_1\}$ ▷ Initialize buffer with first point
Transition Flag $F_{trans} \leftarrow$ False

for each data point d_k in D_{run} (starting from $k = 2$) **do**
    Extract input vector w from d_k
    Compute Next State: $S_{next} \leftarrow \delta(S_{curr}, w)$ ▷ Based on Transition Matrix
    if $S_{next} \neq S_{curr}$ **then** ▷ State Transition Detected
        $F_{trans} \leftarrow$ True
        HANDLETRANSITION($S_{curr}, S_{next}, B_{temp}$) ▷ Process completed event
        Update State: $S_{curr} \leftarrow S_{next}$
        $B_{temp} \leftarrow \{d_k\}$ ▷ Start new event buffer with current point
    else
        Append d_k to B_{temp} ▷ Accumulate data for current state
    end if
end for
HANDLETRANSITION(S_{curr}, NULL, B_{temp}) ▷ Process the final segment
return $\mathcal{E}_{j,g}, \mathcal{E}_{j,k}$

function HANDLETRANSITION($S_{prev}, S_{next}, B_{data}$)
    Let $t_{start} \leftarrow B_{data}[1].t, \quad t_{end} \leftarrow B_{data}[\text{end}].t$
    Calculate Duration: $\tau \leftarrow t_{end} - t_{start}$
    if $\tau < \tau_{min}$ **then**
        return ▷ Discard transient noise
    end if
    if $S_{prev} == q_4$ **then** ▷ Exiting Braking State (q_4)
        Categorize as Braking Event
        Append B_{data} to $\mathcal{E}_{j,g}$ via `on_exit_decelerate()`
    else if $S_{prev} == q_1$ **and** $S_{next} == q_2$ **then** ▷ Exiting Stop (q_1) to Traction (q_2)
        Categorize as Starting Event
        Append B_{data} to $\mathcal{E}_{j,k}$ via `on_exit_accelerate()`
    end if
end function

During the Automatic Train Operation feedback regulation process, brief counter-adjustment signals are frequently issued to balance the rate of change (i.e., control jerk). To prevent the automaton from triggering spurious state transitions caused by this transient sensor noise or fluctuations that do not reflect actual physical state requirements, a filtering mechanism is implemented. To ensure data quality, events with a duration τ shorter than a predefined threshold τ_{min} are classified as transient noise and discarded.

Valid events are categorized based on the predecessor state S_{prev} and successor state S_{next}. For instance, a transition from Dwell (q_1) to Traction (q_2) triggers the `on_exit_accelerate` callback, recording a Starting Event. Conversely, exiting the Braking state (q_4) triggers `on_exit_decelerate`, recording a Braking Event. This mechanism enables the automated and precise identification of key operational phases from continuous datasets.

The event extraction process is described in Algorithm 1.

2.2.3. Dual Definitions of Traction and Braking Time-Series Sets

This study establishes the Startup and Braking Time-series Datasets, which represent the Projection and Restriction of the train's global function $\Psi(t)$ onto specific state intervals. This approach realizes the structured extraction and standardized encapsulation of traction and braking events for the train fleet, providing a data foundation for the subsequent quantitative evaluation and optimization of individual braking processes.

1. Traction Time-Series Dataset Let T_{acc} be defined as the time interval of the train's acceleration state. The k-th acceleration interval is denoted as:

$$T_{acc} = \left\{ \left[t_{start}^{k}, t_{end}^{k} \right] \right\}_{k=1}^{K} \tag{30}$$

By employing a finite state automaton to identify and truncate all acceleration phases within the train operation data, a complete Traction Time-series Dataset, denoted as D_{acc}, is constructed. This dataset records the continuous dynamic trajectory from the moment the train responds to the traction command in a stationary state, begins generating tractive force, until it reaches the target velocity.

$$D_{acc} := \Psi_j(t)\Big|_{T_{acc}} = \left\{ (t, \Psi_j(t)) \;\middle|\; t \in \bigcup_{k=1}^{K} \left[t_{start}^{k}, t_{end}^{k} \right] \right\} \tag{31}$$

2. Braking Time-Series Dataset The finite state automaton reads the train operation status in real-time and identifies the start time t_{start} and end time t_{end} of the braking condition through discrete logic, thereby extracting the braking interval T_{brake}. Assuming a braking event triggers the g-th deceleration state interval, the time interval is recorded as:

$$T_{brake} = \left\{ \left[t_{start}^{g}, t_{end}^{g} \right] \right\}_{g=1}^{G} \tag{32}$$

The braking state data within these intervals are stored in the Braking Time-series Dataset, denoted as D_{brake}. This dataset completely records the continuous evolutionary trajectory of time, position, velocity, and power during the braking process, preserving the differential and integral characteristics of the physical process.

$$D_{brake} := \Psi_j(t)\Big|_{T_{brake}} = \left\{ (t, \Psi_j(t)) \;\middle|\; t \in \bigcup_{g=1}^{G} \left[t_{start}^{g}, t_{end}^{g} \right] \right\} \tag{33}$$

3. Formal Definition of Braking Events Based on the construction of the Braking Time-series Dataset D_{brake}, each independent unit within the dataset is defined as a Braking Event, denoted as $\mathcal{E}_{j,g}$. A braking event acts as an instantiated mapping of control flow logic onto the physical data stream. Bounded by the discrete states of the automaton, it serves as a structured entity encapsulating continuous dynamic behaviors within a specific time window. Through this definition, the continuous operation process is dimensionality-reduced into a finite set of analyzable discrete event objects, providing standardized input units for subsequent energy consumption calculations and strategy optimization.
   - Train Index: Denoted by j, where $j \in \{1, 2, \cdots, N_{train}\}$, representing the j-th train in the fleet.
   - Event Sequence: Denoted by g, where $g \in \{1, 2, \cdots, G_j\}$, representing the g-th braking occurrence for the j-th train.

The Braking Event $\mathcal{E}_{j,g}$ is defined as an instantiated triplet derived from the dataset D_{brake}, comprising the attribution identity, spatiotemporal tags, and physical payload:

$$\mathcal{E}_{j,g} \triangleq \left\langle ID_{train}^{(j)}, T_{brake}^{(j,g)}, \Omega^{(j,g)} \right\rangle \tag{34}$$

- Identity ($ID_{train}^{(j)}$): Explicitly identifies the physical train entity to which the event belongs.
- Occurrence Timestamp ($T_{brake}^{(j,g)}$): Records the absolute timestamp (or the relative start point of operation time) when the braking behavior occurred. It assigns a unique coordinate to the event on the time axis for subsequent temporal correlation analysis.
- Physical Payload ($\Omega^{(j,g)}$): This is the core data entity extracted from the Braking Time-series Dataset. It represents the function restriction of the global state function $\Psi_j(t)$ within the event time window $[t_{start}, t_{end}]$:

$$\Omega^{(j,g)} = \Psi_j(t)\Big|_{t\in[T_{start},T_{end}]} \tag{35}$$

This payload contains continuous trajectories such as velocity $v(t)$, power $P(t)$, and position $s(t)$ during the braking process.

2.3. MPC System Modeling

The Model Predictive Control framework addresses the optimal control problem of regenerative braking energy absorption for a train group within a finite time domain via a receding horizon strategy, as shown in Figure 3. In this diagram, the framework is divided into three functional subsystems distinguished by background colors: the yellow region represents the Integrated Three-Layer Architecture (Data Flow), the blue region denotes the Finite State Automata (Control Flow), and the orange region indicates the Model Predictive Control module (Optimization Decision). Solid arrows illustrate the sequential data transmission between these modules, while the dashed arrow signifies the feedback loop. By applying the optimization results derived from the first braking event in the control sequence to the dwell time of the accelerating trains, the system achieves real-time optimization based on the prediction of future train states.

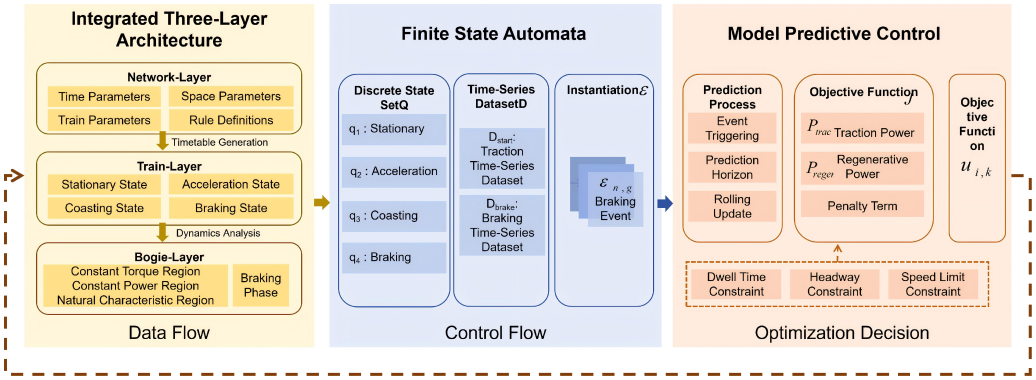

Figure 3. System Framework Diagram.

2.3.1. Energy Overlap Integral and Geometric Alignment Mechanism

To maximize the utilization rate of regenerative braking energy, this study proposes an alignment mechanism based on the geometric characteristics of the power curves for traction and braking trains. Established upon Newton's second law, the longitudinal dynamic equations of the train are formulated to derive the train energy consumption

model. As indicated in Equations (20), (23) and (25), the traction power characteristic $P_{trac}(t)$ exhibits three distinct operational regions:

- Constant Torque Region: Power increases linearly with time.
- Constant Power Region: The power curve is maintained at the peak amplitude (P_{max}), manifesting as a horizontal straight line.
- Natural Characteristic Region: Power decreases inversely as speed increases.

Correspondingly, the regenerative braking power P_{brake} is proportional to the braking speed $v(t)$. Under the assumption of constant deceleration, since $v(t)$ decreases linearly, the braking power $P_{regen}(t)$ exhibits a linear decay over time, forming a triangular profile. Consider a scenario with a braking train g and a set of accelerating trains $\mathcal{K}_{acc}$. To maximize energy absorption, we introduce a dwell time adjustment vector $\boldsymbol{\Delta t} = [\Delta t_1, \ldots, \Delta t_K]^T$, which effectively shifts the traction power curves along the time axis. The Instantaneous Overlap Power $P_{overlap}$ for a specific pair of trains (braking train g and accelerating train k) is defined as:

$$P^{(k,g)}_{overlap}(t, \Delta t_k) = \min\Big(P_{trac,k}(t - \Delta t_k), P_{brake,g}(t)\Big) \tag{36}$$

The total utilized energy $E_{overlap}$ within the overlap time domain Ω is obtained by integrating the effective overlapping power:

$$E_{overlap}(\boldsymbol{\Delta t}) = \int_{t\in\Omega} \min\left(\sum_{k\in\mathcal{K}_{acc}} P_{trac,k}(t - \Delta t_k), P_{brake,g}(t)\right) dt \tag{37}$$

Geometric Alignment Strategy: The energy density of the braking train is highest at the initial phase (peak power P_{brk_peak}). Ideally, this peak should align with the Constant Power Region (P_{max}) of the accelerating train to avoid power saturation or waste. Let t_{brk} denote the braking start time and t_{trac} denote the traction start time. We define the phase delay as $\Delta T = t_{brk} - t_{trac}$. Geometric analysis reveals that the energy utilization function $E(\Delta T)$ possesses piecewise quadratic characteristics. The optimal synchronization occurs when the braking process initiates slightly later than the traction process. Specifically, when $\Delta T \approx t_1$ (where t_1 is the duration of the Constant Torque Region), the "triangular" braking power profile is perfectly embedded into the "trapezoidal" traction power profile, thereby maximizing the overlapping area.

2.3.2. Event-Triggered MPC Framework

To address the geometric misalignment between braking and traction powers, we propose an Event-Triggered MPC framework. This controller operates in a monitoring mode and switches to an optimization mode only when a high-energy regenerative braking event is predicted.

1. State Space and Control Variables
   Trigger Mechanism and Bidirectional Search ScopeTrigger Condition:Let t_{now} denote the current system time. The MPC controller continuously monitors the state of all trains. Upon predicting a regenerative braking event for train g scheduled to start at $t_{brk,g}$, the optimization routine is triggered. The activation instant is determined by advancing the braking time by a look-ahead buffer t_{buffer}:

   $$t_{now} \leq t_{brk,g} - t_{buffer} \tag{38}$$

   Mechanism Principle:Unlike traditional reactive triggers, this mechanism utilizes t_{buffer} (the value is set to match the maximum controllable dwell time window defined by the metro operator) to expand the temporal search scope backwards. By initiating the optimization window prior to the actual braking event, the system creates a wider

feasible solution space. This expanded horizon enables the controller to identify candidate accelerating trains located on both sides of the braking event along the time axis. Consequently, the MPC can achieve perfect energy alignment through bidirectional adjustments:

Delaying Traction: For accelerating trains scheduled before the braking event, the system can extend their dwell times to delay traction.

Advancing Traction: For accelerating trains scheduled slightly after the braking event, the system can reduce their dwell times (subject to t_{dwell}^{min}) to advance traction. This strategy significantly increases the probability of finding an optimal "braking-traction" pair compared to a single-direction adjustment strategy.

Handling of Overlapping Braking Events: To ensure computational feasibility when multiple braking events occur simultaneously, a serialized processing mechanism is adopted. The system treats each braking process as an atomic unit. Events are queued chronologically; in cases of temporal overlap, priority is assigned based on the train departure sequence. The optimization is then executed sequentially, ensuring that valid solutions are found for each train without constraint conflicts.

Prediction Horizon (T_ω): Upon triggering, a prediction horizon $[t_{now}, t_{now} + T_\omega]$ is generated. The length T_ω is designed to cover the complete duration of the braking event, ensuring the optimizer can capture the full energy interaction process. Decision Variables: We define a set of accelerating trains $\mathcal{I}_{acc}$ within the horizon. For each train $i \in \mathcal{I}_{acc}$ scheduled to stop at station k, the decision variable is the dwell time adjustment:

$$\boldsymbol{\Delta t} = [\Delta t_{1,k}, \Delta t_{2,k}, \ldots, \Delta t_{N,k}]^T$$

Adjusting $\Delta t_{i,k}$ shifts the train's subsequent departure time $t_{dep,i,k}$ and physically translates its traction power curve $P_{trac,i}(t)$ along the time axis.

2. Optimization Problem Formulation

The objective is to minimize the net energy drawn from the traction [24] substation (energy conservation) while smoothing power fluctuations (grid stability). The cost function J is formulated as follows:

$$\min_{\boldsymbol{\Delta t}} J = \int_{t_{now}}^{t_{now}+T_\omega} \left(\sum_{i \in \mathcal{I}_{acc}} P_{trac,i}(t, \Delta t_{i,k}) - \eta_{net} \cdot P_{overlap}(t, \boldsymbol{\Delta t}) \right)^2 dt + \lambda \|\boldsymbol{\Delta t}\|_2^2 \quad (39)$$

where:

- Net Power Minimization (First Term):
  $\sum P_{trac,i}$: The total power demand of all accelerating trains in the section.
  $P_{overlap}$: The actual utilized regenerative power (defined in Equation (37)).
  η_{net}: The network transmission efficiency (e.g., 0.95).
  The term implies minimizing the square of the net power supplied by the substation. This quadratic form is chosen to not only reduce total energy consumption but also suppress high-current peaks, thereby reducing Joule heat losses (I^2R) in the feeder network.
- Penalty Term (Second Term):
  λ: A weighting factor balancing energy savings and punctuality.
  $\|\boldsymbol{\Delta t}\|_2^2$: Penalizes excessive changes to the timetable to strictly maintain passenger service quality.

3. Operational Constraints The feasible solution space of the MPC is rigorously bounded by real-world metro operational protocols. Specifically, the optimization is subject to the following hard constraints to guarantee both safety and operational feasibility:

Dwell Time Feasibility The adjusted dwell time t_{dwell}^{new} must remain within the bounds permitted by the operation timetable:

$$t_{dwell}^{min} \leq \left(t_{dwell,i,k}^{original} + \Delta t_{i,k} \right) \leq t_{dwell}^{max} \tag{40}$$

Headway Safety (Anti-Collision) To satisfy the Moving Block signaling requirements, the interval between the arrival of the following train $(i+1)$ and the departure of the preceding train (i) at the same station k must exceed the safe headway H_{safe}:

$$t_{arr,i+1,k} - t_{dep,i,k} \geq H_{safe} \tag{41}$$

Speed Limit Constraint The velocity profile $v_i(t)$ must strictly adhere to the line speed limit $V_{lim}(s)$ at any position s:

$$v_i(t) \leq V_{lim}(s(t)) \tag{42}$$

4. Algorithmic Workflow
The problem is solved using a Receding Horizon Control strategy to handle system stochasticity:
Observation & Filtering: Real-time data acquisition of train states. Braking events with duration $T_{brk} < 10$ s are filtered out as noise to prevent frequent, unnecessary control actions.
Event Prediction: Predict the power profiles of the braking train g and potential accelerating trains $\mathcal{I}_{acc}$ over the horizon T_ω.
Optimization Solving: Solve Equation (39) subject to constraints Equations (40)–(42) to obtain the optimal sequence $\boldsymbol{\Delta t}^*$.
Receding Horizon Actuation:
   - Although a sequence of adjustments is calculated, only the first element $\Delta t_{1,k}^*$ (corresponding to the most immediate train $i = 1$) is executed.
   - This value is sent to the Automatic Train Operation (ATO) system to modify the door closure time.
   - The remaining computed adjustments are discarded.

   Feedback Correction: At the next time step, the system updates the state with new measurements and repeats the optimization. This closed-loop mechanism compensates for model mismatches and external disturbances.
   The primary function of the MPC framework is to leverage the Receding Horizon Control mechanism to predict the energy profiles of accelerating and braking trains, with optimization focusing on the temporal synchronization of energy flows. Meanwhile, variations in physical parameters—such as passenger load fluctuations, traction/braking force limits, and wheel-rail adhesion conditions—are handled by the automatic train control system.

3. Experiments

This section presents extensive experimental results obtained from the simulation platform constructed in our research. To validate the effectiveness of the proposed dynamic scheduling strategy in our platform, multiple comparative experiments were conducted using real-world urban rail transit operational parameters.

The experimental data are referenced from Luoyang Metro Line 1 in China. The simulation system integrates the traction network topology model, the train kinematics model, and the pantograph-catenary electrical model, and generates all simulation parameters

which are used by FSA and MPC. All experimental results are benchmarked against the fixed-timetable scheduling scheme.

3.1. 3D Visualization Analysis of Spatiotemporal Trajectories and Power States

To intuitively visualize the operational status of the train fleet in the spatiotemporal dimension and their corresponding power consumption, a three-dimensional (3D) trajectory map was constructed. Figure 4 illustrates the 3D paths of 10 metro trains (IDs 10101 to 11001) within a continuous time window from 10:00 to 10:10. The three coordinate axes represent time (t), distance (s), and instantaneous power (P), respectively. In the diagram, the colored trajectories illustrate the spatiotemporal movement of the trains, where the geometric undulations reflect changes in power consumption. The specific Train IDs are provided in the legend located at the top-right.

1. Analysis of Figure 4a:
   From the 3D top-down view in Figure 4a, the non-linear progression of the 10 trains across the time and distance dimensions is clearly observable. Each winding curve represents the spatiotemporal trajectory of a train, while the color gradient (mapped to the Z-axis height) reflects the magnitude of the train's current instantaneous power (P).
   - Trajectory Smoothness and Safety: The position-time parameters of all trains strictly conform to the definitions of the train kinematics functions. Furthermore, a strict safety interval is maintained between trajectories in the spatial domain. This demonstrates that the proposed FSA-MPC controller effectively adheres to the safety tracking constraints under the Moving Block System (MBS), ensuring that no tracking conflicts or simulated collisions occur.
   - Discrete Switching of Power States: By observing the morphology of the trajectory lines, it is evident that they are not composed of a single slope but are spliced together from several segments with distinct characteristics. This corresponds to the discrete management of train operational modes by the FSA. The trains switch dynamically among four states: "Stop", "Traction", "Coasting", and "Braking". This state-based control logic ensures the rationality of the train's dynamic behavior at the microscopic level.

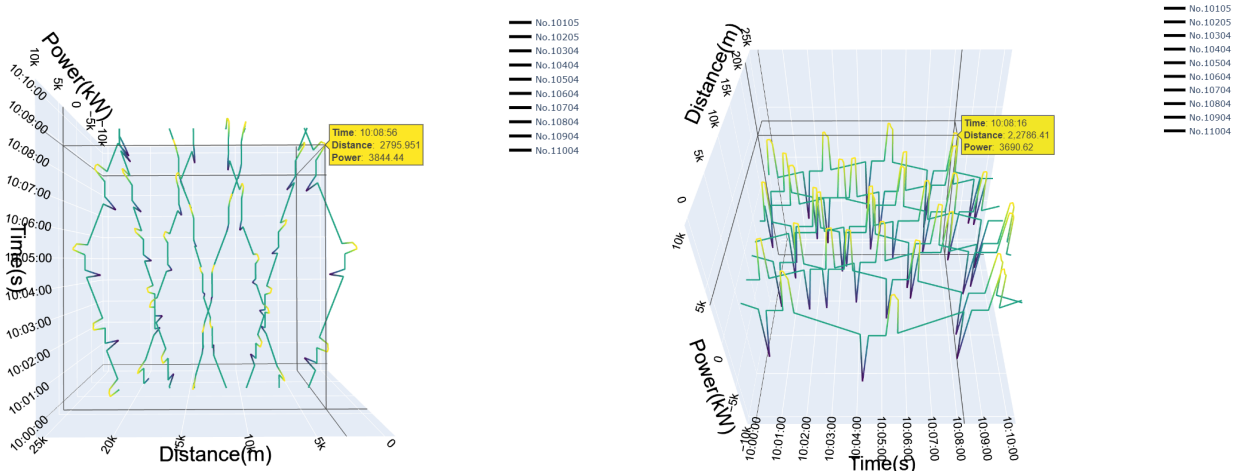

(**a**) Train Travel Path (**b**) Train Operating Power Curve

Figure 4. 3D Train Operating Power Curve.

2. Analysis of Figure 4b:
   Figure 4b provides an alternative perspective, focusing on the magnitude of power variations. The Z-axis visually quantifies the power values.

- Distribution Characteristics of Power Peaks: The prominent yellow peaks in the figure represent trains in the high-power traction state, while the deep blue valleys extending downward represent trains in the regenerative braking state.
- Stochasticity in Non-optimized States: Prior to the optimization by the proposed algorithm, the distribution of these yellow peaks (traction) and blue valleys (braking) along the time axis exhibits significant non-effective overlapping. This phenomenon is the root cause of RBE wastage—specifically, when a train is at a "blue braking valley," neighboring trains are frequently not at a "yellow traction peak," resulting in the inability to absorb the generated energy. Figure 4 graphically reveals this spatiotemporal mismatch between energy supply and demand in the existing system.

3.2. Comparative Analysis of Traction and Braking Power Curves Before and After Optimization

To quantitatively evaluate the effectiveness of the proposed dynamic scheduling strategy in terms of spatiotemporal energy synchronization, the aggregate traction and braking power profiles were extracted for the interval 10:00:00–10:10:00. These profiles were obtained by separately summing the power of all trains in the traction phase and all trains in the braking phase at each time instant.

1. Analysis of Figure 5a:
   Figure 5a illustrates the traction power curves (Green, Positive Power) and braking power curves (Red, Negative Power) for all trains under the unoptimized scenario (i.e., adhering to the traditional fixed timetable). It is clearly observable that the occurrence times of the red curves (braking energy generation) and the green curves (traction energy demand) are frequently misaligned. To facilitate observation, typical regions of interest are highlighted with blue boxes. For instance, near 10:02:30, a substantial traction energy peak (Green) occurs, but the corresponding braking power (Red) is at a valley. This indicates that at that particular moment, the renewable energy in the power grid was not properly matched.
2. Analysis of Figure 5b:
   Figure 5b presents the results following the application of the proposed FSA-MPC dynamic scheduling strategy. In sharp contrast to Figure 5b, nearly every valley of the red braking curve in Figure 5a aligns with an upward peak of the green traction curve. This alignment is not coincidental but is the direct result of the predictive regulation by the MPC controller. When the system predicts that a specific train is about to enter a station and brake, the FSA scheduler finely adjusts the departure time of a neighboring train, ensuring it enters the acceleration phase simultaneously.

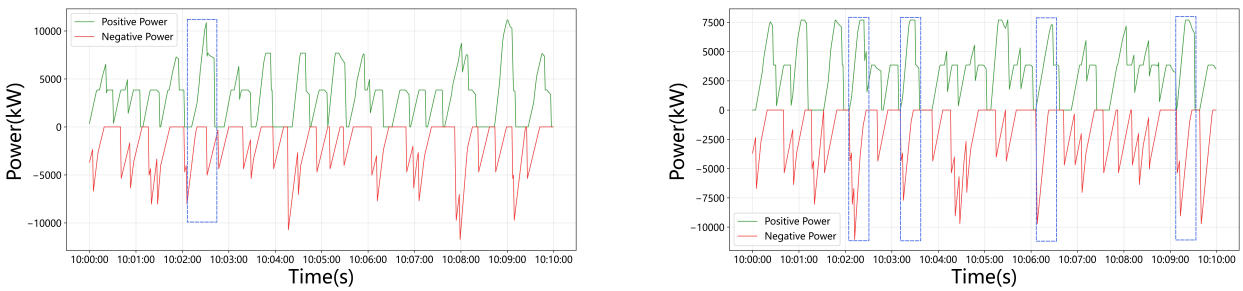

(**a**) Pre-optimization (**b**) Post-optimization

Figure 5. Separate Presentation of Traction and Braking Energy.

3.3. Net Power Profile and Grid Impact Assessment

Furthermore, by algebraically superimposing the instantaneous power of all operating trains, the net power profile from the perspective of the traction substation is obtained.

1. Analysis of Figure 6a:
   Figure 6 depicts the net power profile of the system prior to optimization. The curve exhibits extreme volatility, frequently oscillating between high positive values (exceeding +10,000 kW) and deep negative values (below −10,000 kW).The severe power ramp rate poses a threat to the lifespan of power supply equipment and simultaneously escalates operational costs, specifically the Demand Charge imposed by utility companies.
2. Analysis of Figure 6b:
   Figure 6 illustrates the net power profile following the implementation of the proposed optimization strategy. A comparative analysis reveals a marked reduction in both the amplitude and duration of the negative power peaks below the zero axis. The originally prominent negative intervals have been effectively offset by the traction demands of other trains. Although the peak traction power persists, the power fluctuation range has narrowed to ±7500 kW.

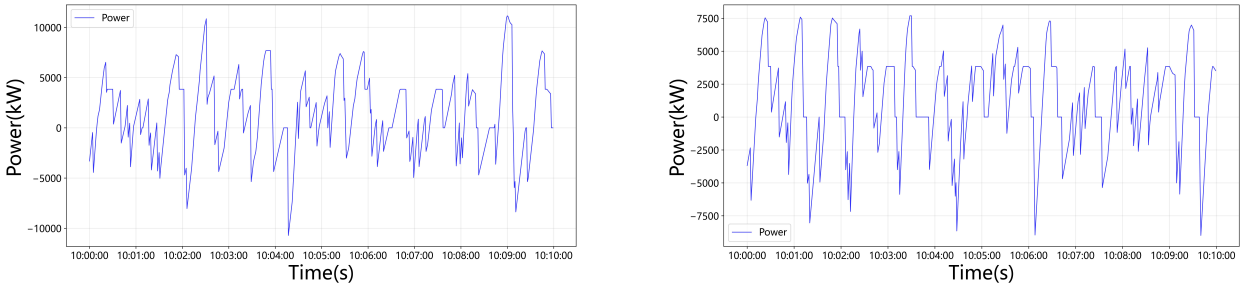

(**a**) Pre-optimization (**b**) Post-optimization

Figure 6. Train Energy Consumption.

3.4. Verification of the Energy Synchronization Mechanism During a Typical Braking Event

To elucidate the execution mechanism of the FSA-MPC scheduling strategy, this study analyzes the power interaction details between Train 10804 (in traction state) and Train 10504 (in braking state) within the time window from 10:04:00 to 10:04:45. The Figure 7 contrasts the traction curve variations before and after the optimization operation, as well as their matching relationship with the braking curve.Specifically, in Figure 7c, the blue curve represents the braking power profile of the supplier train (No. 10504), while the orange curves depict the traction power profiles of the recipient train (No. 10804).

Figure 7 details the regenerative braking energy absorption between Train No. 10804 and Train No. 10504 before and after the schedule adjustment. Prior to optimization(indicated by the dashed orange line), a "temporal mismatch" was observed, wherein the potential recipient (the accelerating train) completed its acceleration phase just before the supplier train initiated braking. To address this, the FSA-MPC controller delayed the departure of Train No. 10804 by 10 s (shifted from the dashed line to the solid orange line), subject to dwell time constraints. This time-shift operation effectively aligned the high-power "Traction Plateau" with the supplier's "Braking Peak." Consequently, the absorption of instantaneous regenerative energy was optimized, thereby validating the precision of the proposed scheduling strategy.

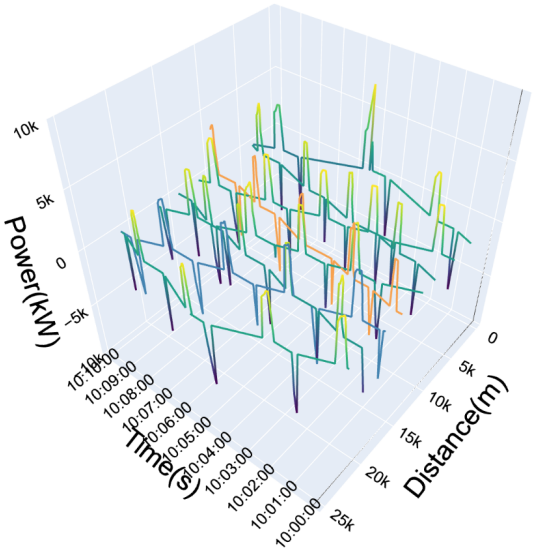

(**a**) Multi-train System

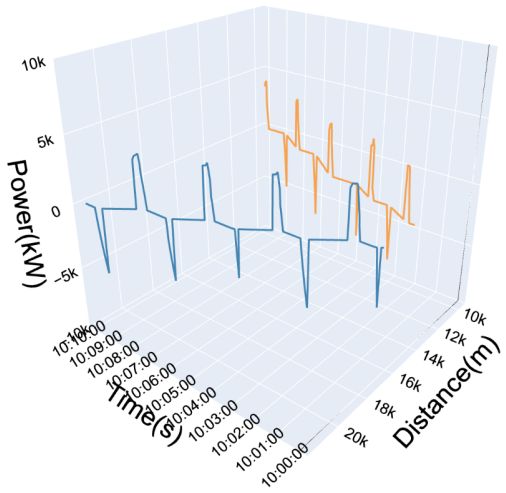

(**b**) An Accelerating-braking Train Pair

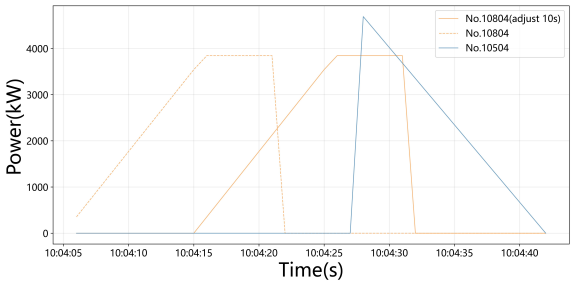

(**c**) A Braking Event

Figure 7. Cooperative Energy Exchange Event.

3.5. Experimental Results on Energy Efficiency

To quantitatively evaluate the energy-saving performance of the proposed scheduling algorithm, this study establishes core metric based on the physical graph model: the Regenerative Energy Utilization Rate.

Based on the definitions provided earlier, let $E_{release}$ represent the energy fed back during the braking process. For a braking train g and a set of accelerating trains $\mathcal{K}_{acc}$, the total utilized energy within the overlapping time domain Ω is defined as the effective overlapping energy, denoted as $E_{overlap}$.

Regenerative Energy Utilization Rate (η_{RBE}): This metric measures the proportion of regenerative energy generated during braking that is effectively utilized by accelerating trains within an operation cycle. It is calculated as the ratio of the effective overlapping energy to the total feedback energy. The formula is expressed as follows:

$$\eta_{RBE} = \frac{E_{overlap}}{E_{release}} \times 100\%$$

1. Analysis of Braking Utilization Stability
   The temporal distribution of regenerative braking energy utilization is illustrated in Figure 8. The scatter plot contrasts the utilization rates of the original schedule (represented by red markers) against the optimized schedule (green markers) throughout the simulation period.
   As observed in Figure 8, the original schedule exhibits a high degree of stochasticity, with a significant density of braking events clustering in the low-utilization region

(0–20%). This indicates a frequent mismatch between braking trains and accelerating trains on the catenary network, leading to substantial energy wastage in the braking resistors.

In contrast, the optimized schedule demonstrates a marked shift in distribution. A distinct clustering of events is visible in the 50–60% utilization range (e.g., trains 10202 10502, and 10802 consistently achieving >54%). While zero-utilization events still occur due to inherent network constraints (e.g., lack of simultaneous traction demand), the optimization algorithm successfully shifts the mean utilization rate from 67.03% in the baseline scenario to 78.43% in the optimized scenario. This represents a relative improvement of 12.4% in average braking efficiency, validating the algorithm's effectiveness in synchronizing train timetables to maximize overlap phases.

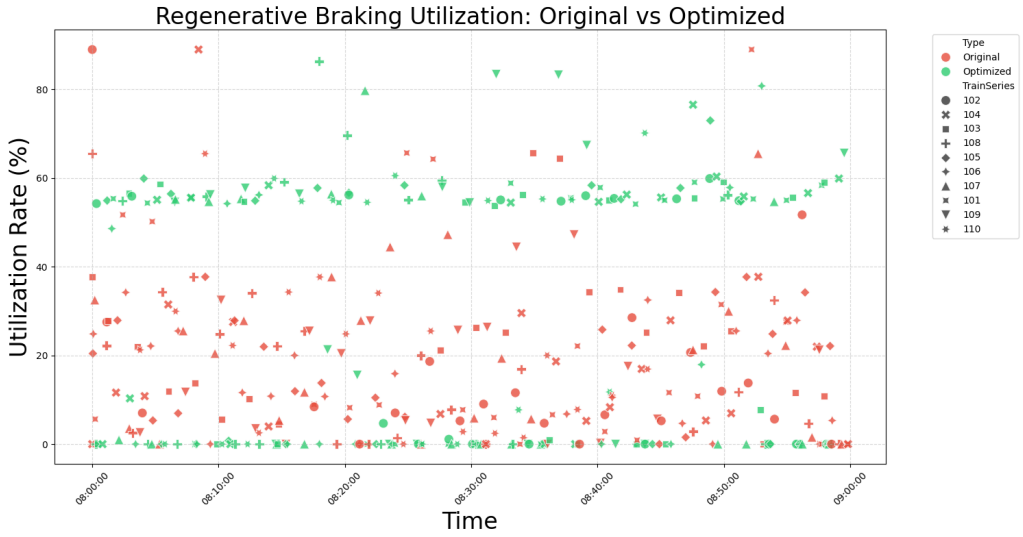

Figure 8. Comparison of utilization rate distribution over time.

2. Quantitative Comparison of Absorbed Energy

Figure 9 presents the aggregate absorbed regenerative energy for each train, providing a train-level perspective on the optimization benefits. The green bars (Optimized) consistently surpass the red bars (Original) across the majority of the fleet.

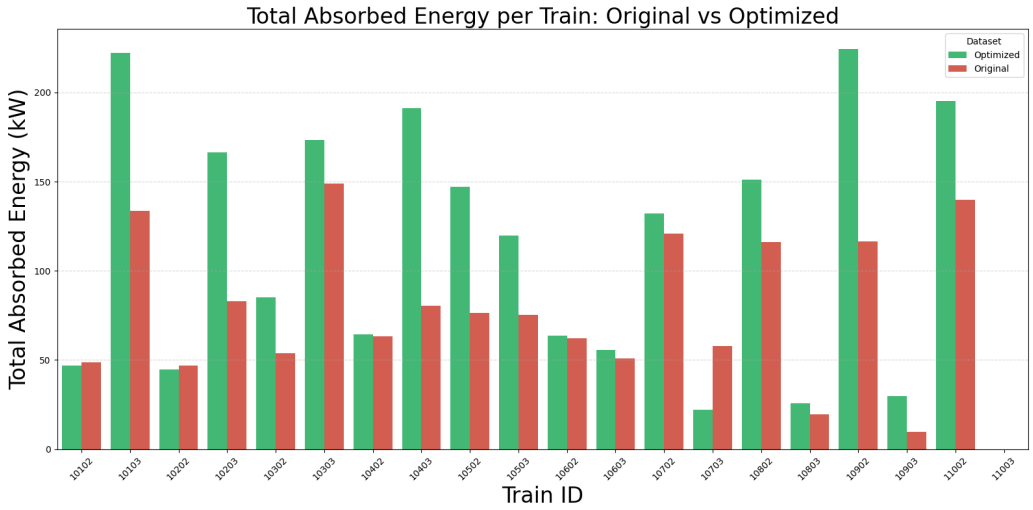

Figure 9. Comparison of total absorbed energy per train.

Notably, certain trains (e.g., Train 10403 and Train 10902) exhibit dramatic improvements in energy absorption. For instance, in the original schedule, several trains

operated with minimal grid receptivity, whereas the optimized schedule enabled these specific trains to feed back significant energy into the grid. This result confirms that the proposed optimization strategy does not merely improve the global average but effectively addresses local inefficiencies for individual train services, leading to a more balanced and energy-efficient metro operation.

4. Discussion

Based on the experimental results presented above, this study further elucidates the underlying mechanisms of energy efficiency improvement, the technical advantages of the proposed method, and its potential impact on existing urban rail transit systems.

4.1. Mechanism of Energy Interaction Under the "Train-Network-Control" Three-Layer Coupled Architecture

Existing literature often simplifies train energy conservation into a single-train speed profile optimization problem or focuses on macroscopic timetable adjustments, frequently neglecting the constraints imposed by bottom-level electrical physical characteristics. The experimental results (specifically Figure 2) underscore the necessity of constructing a "Train-Network-Control" three-layer physical simulation system.

1. Necessity of Physical Coupling:
   The optimization effects on train power curves observed in the experiments directly benefit from the precise modeling of train operational characteristics within the simulation system. The proposed three-layer architecture ensures both the logical feasibility of dispatching commands and the physical validity of the electrical network structure.
2. Transition to Active Energy Management:
   The energy overlap demonstrated in Figure 5 validates the system's transformation from "passive reception" to "active management." In traditional modes, the power grid acts merely as a passive energy carrier. In contrast, under the FSA-MPC framework, the controller proactively adjusts train operating conditions by predicting future risks of voltage limit violations, thereby enabling active energy regulation.

4.2. The Effectiveness of FSA in Complex Control Problems

Train operation control is intrinsically a Hybrid System problem, comprising continuous dynamic equations (e.g., speed, displacement) and discrete logical states (e.g., traction, coasting, braking). Directly employing nonlinear MPC to solve such problems often leads to computational explosion, making it difficult to meet real-time requirements. The hybrid automaton model introduced in this paper plays a pivotal role in resolving this contradiction.

1. Discrete Abstraction of Continuous States:
   By abstracting the train operation process into a finite state flow graph (as illustrated in Figure 2), the FSA compresses the infinite-dimensional continuous control space into a finite-dimensional sequence of modes. This eliminates the need for the controller to search the entire space for nonlinear solutions at every step, transforming the problem into a parameter optimization task under specific, constrained modes.
2. Internalization of Logical Constraints:
   The FSA structure is naturally suited for handling hard logical constraints in rail transit, such as "dwelling time within constraint ranges" or "maintaining safe separation between preceding and following trains." While these constraints are often difficult to formulate in pure mathematical programming, they are naturally translated into state transition conditions within the automaton model.

4.3. Analysis of Robust Mechanism Against Stochastic Disturbances

Urban rail transit systems operate in typical high-density environments subject to strong disturbances. Fluctuations in passenger boarding/alighting times and minor delays in signaling systems can disrupt pre-scheduled energy-saving timetables. The robustness demonstrated by the proposed method is primarily attributed to the integration of the MPC rolling horizon mechanism and event-triggered strategies.

1. Rolling Horizon and Feedback Correction:
   The core of MPC lies in the principle of "Receding Horizon Control." The controller not only calculates the control input based on the current state $x(t)$ but also predicts the state trajectory for the future N steps. When external disturbances cause the actual state to deviate from the predicted value, the optimization problem in the next control cycle automatically replans based on the updated real-time state. This closed-loop feedback mechanism effectively "absorbs" errors, pulling the system back to the optimal trajectory and preventing error accumulation.
2. Event-Triggered Dynamic Reconfiguration:
   The FSA designed in this paper introduces a triggering mechanism based on "Braking Events." Once a specific train brakes earlier or later than expected due to a fault or delay, the system immediately triggers a new global optimization to dynamically adjust the traction schedules of adjacent trains. This mechanism enables the rapid reorganization of the energy transmission network after disturbances occur, rather than rigidly executing an invalidated plan.

4.4. Limitations of the Study

Although this study validates the theoretical effectiveness of the dynamic scheduling method in energy conservation, certain limitations remain regarding its translation into practical engineering applications:

1. Simplification of Physical Modeling:
   The current research assumes that regenerative braking energy within the same power supply section can be transmitted instantaneously and losslessly. However, actual DC traction networks possess significant line resistance. As the distance between trains increases, heat losses during transmission increase. The absence of a position-dependent impedance model leads to a failure to account for energy dissipation caused by long-distance transmission, thereby resulting in an overestimation of the actual energy utilization rate in the simulation.
2. Absence of Multi-objective Synergistic Optimization:
   The current control strategy primarily focuses on minimizing energy consumption, without exploring the nonlinear trade-offs between energy consumption, punctuality, and passenger comfort. In actual operations, algorithms strictly prioritizing energy matching may generate train schedules that compromise the passenger experience.

5. Conclusions

This study proposes and validates an optimization methodology for enhancing regenerative braking energy utilization in urban rail transit systems through collaborative train scheduling. By analyzing the three-dimensional spatiotemporal trajectories and power distribution of multiple trains, the following conclusions are drawn:

1. Synchronization of Traction and Braking:
   The method successfully synchronizes the traction and braking phases of adjacent trains. Visual comparisons of power curves before and after optimization confirm a significant increase in the overlap between motoring and braking intervals.

2. Realization of Direct Energy Exchange:
   Direct energy exchange between trains is effectively achieved. Detailed analysis of specific time windows indicates that the high-power energy bursts generated by braking trains are immediately absorbed by accelerating trains, thereby reducing the demand on grid power.
3. Reduction in Net Substation Energy Consumption:
   The overall net energy consumption of the traction power supply system is significantly reduced. The optimized net power curve demonstrates lower total energy consumption and reduced peak power demand compared to the unoptimized baseline schedule.

This study establishes a theoretical foundation and technical pathway for the construction of next-generation green and intelligent rail transit systems, focusing on deep evolution in the following three core directions:

- Multi-Objective Dynamic Synergistic Optimization: Future work will seek a dynamic weight optimization mechanism based on nonlinear game theory to achieve optimal balance between passenger experience and system energy consumption, ensuring operational efficiency is maintained.
- Physically Perceptive Modeling: To address the limitations of existing research regarding grid physical characteristics, future models will incorporate line impedance and distance attenuation in regenerative energy transmission. This constitutes the immediate next step for our research group. This will quantify the impact of distance on energy loss, upgrading energy-saving scheduling from simple "temporal overlap" to "spatiotemporal precise matching," ensuring the effectiveness of scheduling strategies at the electrical physical level.
- Hierarchical Global Optimization Architecture: A hybrid "Data-Driven + Model-Driven" architecture combining Deep Reinforcement Learning (DRL) will be constructed. This will allow an upper-layer Agent to utilize historical operational data to learn traffic evolution patterns and proactively adjust the parameters of the lower-layer MPC (such as weighting factors and constraint boundaries), thereby enhancing the system's adaptability in unstructured environments.

In summary, the dynamic scheduling method proposed in this paper not only theoretically proves the feasibility of algorithmic improvements in regenerative braking energy efficiency but also provides a tangible and viable solution for building a low-carbon, efficient, and intelligent urban rail transit network.

Author Contributions: Conceptualization, Y.X. and Y.Z.; methodology, Y.X.; software, Y.X. and W.X.; validation, Y.X. and W.X.; formal analysis, Y.X. and Y.Z.; investigation, Y.X.; resources, W.S.; data curation, Y.X.; writing—original draft preparation, Y.X. and Y.Z.; writing—review and editing, W.S. and Y.Z.; visualization, W.X.; supervision, W.S.; project administration, Y.Z.; funding acquisition, W.S. All authors have read and agreed to the published version of the manuscript.

Funding: This research was funded by the Key Scientific and Technological Project of Henan Province, grant number 242102241065, and supported by the Henan Engineering Research Center of Rail Transit Operation Safety and Transport Efficiency Technology and Application.

Institutional Review Board Statement: Not applicable.

Informed Consent Statement: Not applicable.

Data Availability Statement: The data presented in this study are available from the first author upon request.

Conflicts of Interest: The authors declare no conflicts of interest.

References

1. The Transport Politic. Transit Project Openings in 2025: A Global Review. 2025. Available online: https://www.thetransportpolitic.com/2025/01/12/transit-project-openings-in-2025-a-global-review/ (accessed on 10 December 2025).
2. Deng, L.; Tang, S.; Chen, M.; Zhang, Y.; Tian, Y.; Chen, Q. Energy-Efficient Optimization Method for Timetable Adjusting in Urban Rail Transit. *Mathematics* **2025**, *13*, 2119. [CrossRef]
3. Alnuman, H.; Gladwin, D.; Foster, M. Electrical Modelling of a DC Railway System with Multiple Trains. *Energies* **2018**, *11*, 3211. [CrossRef]
4. Qin, B.; Liu, J.; Wang, H.; Wang, Z.; Xiong, Z.; Wang, M.; Qian, Q. Energy-efficient and reliable urban rail transit: A new framework incorporating underground energy storage systems. *iEnergy* **2025**, *4*, 86–97. [CrossRef]
5. Barrero, R.; Tackoen, X.; Van Mierlo, J. Stationary or onboard energy storage systems for energy consumption reduction in a metro network. *Proc. Inst. Mech. Eng. F J. Rail Rapid Transit* **2010**, *224*, 207–225. [CrossRef]
6. Szeląg, A.; Jefimowski, W.; Maciołek, T.; Nikitenko, A.; Wieczorek, M.; Lewandowski, M. Hybrid Energy Storage System for Regenerative Braking Utilization and Peak Power Decrease in 3 kV DC Railway Electrification System. *Electronics* **2025**, *14*, 1752. [CrossRef]
7. Chen, M.; Xiao, Z.; Sun, P.; Wang, Q.; Jin, B.; Feng, X. Energy-Efficient Driving Strategies for Multi-Train by Optimization and Update Speed Profiles Considering Transmission Losses of Regenerative Energy. *Energies* **2019**, *12*, 3573. [CrossRef]
8. Xue, J.; Zhuang, K.; Zhao, T.; Zhang, M.; Qiao, Z.; Cui, S.; Gao, Y. Speed Tracking Control of High-Speed Train Based on Particle Swarm Optimization and Adaptive Linear Active Disturbance Rejection Control. *Appl. Sci.* **2022**, *12*, 10558. [CrossRef]
9. Kabra, A.; Mitsch, S.; Platzer, A. Verified Train Controllers for the Federal Railroad Administration Train Kinematics Model: Balancing Competing Brake and Track Forces. *IEEE Trans. Comput.-Aided Des. Integr. Circuits Syst.* **2022**, *41*, 4067–4078. [CrossRef]
10. Rochard, B.P.; Schmid, F. A review of methods to measure and calculate train resistances. *Proc. Inst. Mech. Eng. F J. Rail Rapid Transit* **2000**, *214*, 185–199. [CrossRef]
11. Heineken, W.; Richter, M.; Birth-Reichert, T. Energy-Efficient Train Driving Based on Optimal Control Theory. *Energies* **2023**, *16*, 6712. [CrossRef]
12. Li, L.; Dong, W.; Ji, Y.; Zhang, Z.; Tong, L. Minimal-Energy Driving Strategy for High-Speed Electric Train with Hybrid System Model. *IEEE Trans. Intell. Transp. Syst.* **2013**, *14*, 1642–1653. [CrossRef]
13. Lv, J.; Lu, W.; Luo, Z.; Ahmad, E.; Lv, J. Safety-Oriented Distance Control for Train Platoon Under Actuator Delays: A Reachability and Hybrid H_2/H_∞ Framework. *IET Intell. Transp. Syst.* **2025**, *19*, e70105. [CrossRef]
14. Chai, M.; Wang, H.; Tang, T.; Liu, H.; Chai, J.; Liu, H. A Relative Operation-Based Separation Model for Safe Distances of Virtually Coupled Trains. *IEEE Trans. Intell. Veh.* **2024**, *9*, 2031–2045. [CrossRef]
15. Basile, D.; Di Giandomenico, F.; Gnesi, S. Statistical Model Checking of an Energy-Saving Cyber-Physical System in the Railway Domain. In Proceedings of the 32nd ACM/SIGAPP Symposium on Applied Computing, Marrakech, Morocco, 3–7 April 2017; pp. 1356–1363. [CrossRef]
16. Luteberget, B.; Claessen, K.; Johansen, C. Design-Time Railway Capacity Verification using SAT modulo Discrete Event Simulation. In Proceedings of the 2018 Formal Methods in Computer Aided Design (FMCAD), Austin, TX, USA, 30 October–2 November 2018; pp. 1–9. [CrossRef]
17. ShangGuan, W.; Chen, J.Q.; Li, B.; Guo, L.N.; Li, M.; Chen, L.Y. Simulation of a high-speed train control system based on High Level Architecture and its credibility analysis. In *Proceedings of the WIT Transactions on The Built Environment*; WIT Press: Billerica, MA, USA, 2010; Volume 114, pp. 535–546. [CrossRef]
18. Ding, F.; Zhu, H.; Wang, F.; Sun, X.; Lin, S.; He, Z. Evaluation of Voltage Quality and Energy Saving Benefits of Urban Rail Transit Power Supply Systems Considering the Access of Photovoltaics. *CSEE J. Power Energy Syst.* **2023**, *9*, 2309–2320. [CrossRef]
19. Golightly, D.; Bhattacharyya, A.; Pierce, K.; Tian, Z.; Lyu, X.; Jiang, K.; Liu, X. Applying Collaborative Co-Simulation to Railway Traction Energy Consumption. *Electronics* **2025**, *14*, 1467. [CrossRef]
20. Josyula, S.P.; Törnquist, J.; Lundberg, L. Parallel Computing for Multi-Objective Train Rescheduling. *IEEE Trans. Emerg. Top. Comput.* **2020**, *8*, 1016–1032. [CrossRef]
21. Long, S.; Meng, L.; Wang, Y.; Luan, X.; Zhang, P. A Bi-objective Integrated Optimization Model of High-speed Train Rescheduling and Train Control. *J. Transp. Syst. Eng. Inf. Technol.* **2020**, *20*, 163–169.
22. Zhao, Y. Optimization Model Design of Regenerative Braking Energy Utilization of Subway Train based on Block Zoning. In Proceedings of the 6th International Conference on Energy Science and Applied Technology (ESAT 2021), Yichang, China, 29–30 May 2021; Volume 804, p. 032002.
23. Deng, L.; Chen, M.; Duan, K.; Li, O.; Shi, F. Integrated energy-efficient optimization for urban rail transit timetable. *IET Intell. Transp. Syst.* **2023**, *17*, 1750–1764. [CrossRef]
24. Bai, Y.; Cao, Y.; Yu, Z.; Ho, T.K.; Roberts, C.; Mao, B. Cooperative control of metro trains to minimize net energy consumption. *IEEE Trans. Intell. Transp. Syst.* **2020**, *21*, 2063–2077. [CrossRef]

25. Zhang, H.; Zhang, J.; Zhou, L.; Xiong, P.; Zhao, Z. Hierarchical Operation Optimization for Regenerative Braking Energy Utilizing in Urban Rail Traction Power Supply System. *Energies* **2023**, *16*, 7268. [CrossRef]
26. Ramos, A.; Pena, M.T.; Fernández, A.; Cucala, P. Mathematical Programming Approach to Underground Timetabling Problem for Maximizing Time Synchronization. *Dir. Organ.* **2007**, *35*, 38–52. [CrossRef]
27. Yang, X.; Chen, A.; Li, X.; Ning, B.; Tang, T. An energy-efficient scheduling approach to improve the utilization of regenerative energy for metro systems. *Transp. Res. C Emerg. Technol.* **2015**, *57*, 13–29. [CrossRef]
28. Ran, X.C.; Chen, S.K.; Liu, G.H.; Bai, Y. Energy-efficient approach combining train speed profile and timetable optimisations for metro operations. *IET Intell. Transp. Syst.* **2020**, *14*, 1831–1841. [CrossRef]
29. da Silva, M.T.; Bitarães, S.M.; Yamashita, A.S.; Torre, M.P.; Moreira, V.d.S.; Euzébio, T.A.M. Centralized Finite State Machine Control to Increase the Production Rate in a Crusher Circuit. *Energies* **2024**, *17*, 3374. [CrossRef]
30. Hu, Z.; Ma, R. Adaptive event-triggered tracking control via switching functions. *Automatica* **2025**, *171*, 112813. [CrossRef]
31. Yang, S.; Liao, F.; Wu, J.; Timmermans, H.J.; Sun, H.; Gao, Z. A bi-objective timetable optimization model incorporating energy allocation and passenger assignment in an energy-regenerative metro system. *Transp. Res. B Methodol.* **2020**, *133*, 85–113. [CrossRef]
32. Yang, X.; Chen, A.; Wu, J.; Gao, Z.; Tang, T. An energy-efficient rescheduling approach under delay perturbations for metro systems. *Transp. B Transp. Dyn.* **2019**, *7*, 386–400. [CrossRef]
33. Li, W.; Jiang, S.; Jin, M. Multi-Objective Optimization and Weight Selection Method for Heavy Haul Trains Trajectory. *IEEE Access* **2022**, *10*, 41152–41162. [CrossRef]
34. Lukaszewicz, P. Running resistance and energy consumption of ore trains in Sweden. *Proc. Inst. Mech. Eng. F J. Rail Rapid Transit* **2009**, *223*, 189–197. [CrossRef]
35. Ding, Y.; Zhou, F.; Bai, Y.; Li, R. A correction model of loaded train's grade resistance calculation. In Proceedings of the 5th Advanced Forum on Transportation of China (AFTC 2009), Beijing, China, 17 October 2009; pp. 267–271. [CrossRef]
36. Szűcs, M.M.; Zábori, Z. Investigation into resistance forces from the wheel-rail interface of a four-axle railway vehicle in curved track. *J. Theor. Appl. Mech.* **2025**, *63*, 647–656. [CrossRef]
37. Niu, J.; Sui, Y.; Yu, Q.; Cao, X.; Yuan, Y. Aerodynamics of railway train/tunnel system: A review of recent research. *Energy Built Environ.* **2020**, *1*, 351–375. [CrossRef]
38. Scheepmaker, G.M.; Goverde, R.M.; Kroon, L.G. Energy-efficient train control methods: A review. *Transp. Res. Part C Emerg. Technol.* **2017**, *75*, 412–442. [CrossRef]
39. Wang, P.; Goverde, R.M. Multi-train trajectory optimization for energy-efficient timetabling. *Eur. J. Oper. Res.* **2017**, *261*, 621–633. [CrossRef]
40. Zhang, N.; Wu, Z.; Gao, C.; Tang, T. An optimal train speed profile planning method for induction motor traction system. *Energies* **2021**, *14*, 5153. [CrossRef]
41. Wang, P.; Goverde, R.M. Multiple-phase train trajectory optimization with signalling and operational constraints. *Transp. Res. C Emerg. Technol.* **2016**, *69*, 255–275. [CrossRef]
42. Feng, J.; Ye, Z.; Wang, C.; Xu, M.; Labi, S. An Integrated Optimization Model for Energy Saving in Metro Operations. *IEEE Trans. Intell. Transp. Syst.* **2019**, *20*, 3059–3069. [CrossRef]
43. Miyatake, M.; Ko, H. Optimization of train speed profile for minimum energy consumption. *IEEJ Trans. Electr. Electron. Eng.* **2010**, *5*, 263–269. [CrossRef]
44. Gonzalez-Gil, A.; Palacin, R.; Batty, P. Sustainable urban rail systems: Strategies and technologies for optimal management of regenerative braking energy. *Energy Convers. Manag.* **2014**, *75*, 374–388. [CrossRef]

Disclaimer/Publisher's Note: The statements, opinions and data contained in all publications are solely those of the individual author(s) and contributor(s) and not of MDPI and/or the editor(s). MDPI and/or the editor(s) disclaim responsibility for any injury to people or property resulting from any ideas, methods, instructions or products referred to in the content.